Warm-fluid stability properties of intense non-neutral charged particle beams with pressure anisotropy

Ronald C. Davidson and Sean Strasburg
Plasma Physics Laboratory, Princeton University, Princeton, New Jersey 08543

(Received 28 January 2000; accepted 29 February 2000)

The macroscopic warm-fluid model developed by Lund and Davidson [Phys. Plasmas **5**, 3028 (1998)] is used in the smooth-focusing approximation to investigate detailed electrostatic stability properties of an intense charged particle beam with pressure anisotropy. The macroscopic fluid-Maxwell equations are linearized for small-amplitude perturbations, and an eigenvalue equation is derived for the perturbed electrostatic potential $\delta\phi(\mathbf{x},t)$, allowing for arbitrary anisotropy in the perpendicular and parallel pressures, $P_\perp^0(r)$ and $P_\parallel^0(r)$. Detailed stability properties are calculated numerically for the case of extreme anisotropy with $P_\parallel^0(r)=0$ and $P_\perp^0(r)\neq 0$, assuming axisymmetric wave perturbations ($\partial/\partial\theta=0$) of the form $\delta\phi(\mathbf{x},t)=\delta\hat{\phi}(r)\exp(ik_z z-i\omega t)$, where k_z is the axial wavenumber, and $Im\,\omega>0$ corresponds to instability (temporal growth). For $k_z=0$, the analysis of the eigenvalue equation leads to a discrete spectrum $\{\omega_n\}$ of stable oscillations with $Im\,\omega_n=0$, where n is the radial mode number. On the other hand, for sufficiently large values of $k_z r_b$, where r_b is the beam radius, the analysis leads to an anisotropy-driven instability ($Im\,\omega>0$) provided the normalized Debye length ($\Gamma_D=\lambda_{D\perp}/r_b$) is sufficiently large and the normalized beam intensity ($s_b=\hat{\omega}_{pb}^2/2\gamma_b^2\omega_{\beta\perp}^2$) is sufficiently below the space-charge limit. Depending on system parameters, the growth rate can be a substantial fraction of the focusing frequency $\omega_{\beta\perp}$ of the applied field. © *2000 American Institute of Physics.* [S1070-664X(00)02506-4]

I. INTRODUCTION

There is increasing interest in the equilibrium and stability properties of intense charged particle beams,[1–5] with potential applications[6–10] including heavy ion fusion, transmutation of radioactive waste, accelerator-based production of tritium, and spallation neutron sources. At the beam intensities of practical interest, it is particularly important to develop an improved theoretical understanding of the influence of space-charge effects and collective processes on detailed stability and transport properties.[11–39] In general, a complete description of collective processes in intense non-neutral beams requires a knowledge of the beam distribution function $f(\mathbf{x},\mathbf{p},t)$ in the six-dimensional phase space $(\mathbf{x},\mathbf{p})$, in order to carry out numerical simulations using the distribution function as an initial condition, or to carry out analytical studies of kinetic equilibrium and stability behavior. While considerable progress has been made in analytical investigations based on the Vlasov–Maxwell equations,[11–31,40] such kinetic analyses are often complex, even under idealized assumptions. It is therefore important to develop and test the robustness of alternative theoretical models, such as macroscopic models[41–51] based on the fluid-Maxwell equations, for investigating beam equilibrium and stability properties. Such macroscopic fluid descriptions have met with recent success in describing the propagation of space-charge-dominated (low-emittance) beams in periodic-focusing transport systems,[48,51] and in describing high-frequency collective oscillations in high-intensity beams.[50] In the present paper, we make use of the macroscopic warm-fluid model developed by Lund and Davidson[50] in the smooth-focusing approximation to investigate the linear stability properties of an intense charged particle beam, allowing for equilibrium pressure anisotropy ($P_\perp^0\neq P_\parallel^0$). A particular focus in the present analysis is application of the warm-fluid model to investigate the anisotropy-driven ($P_\perp^0>P_\parallel^0$) instability observed by Lund *et al.*[37–39] in particle-in-cell simulations and studied analytically using the Vlasov–Maxwell equations. Such anisotropies are well known to develop naturally in accelerators. For example, for a beam of charged particles of mass m and charge q that is accelerated through a voltage V, a simple estimate shows that the final and initial longitudinal temperatures (in energy units) are related[4] in the nonrelativistic case by $T_{\parallel f}=T_{\parallel i}^2/2qV$. In the relativistic case, this relation is modified to become $T_{\parallel f}=T_{\parallel i}^2\gamma_i^3/\beta_f^2\gamma_f^3 mc^2$, where γ is the relativistic mass factor and β is the relativistic velocity. As an example, for an electron beam with initial energy 10 keV and temperature $T_{\parallel i}=0.5$ eV accelerated to 1 MeV, the final longitudinal temperature is $T_{\parallel f}=2.1\times 10^{-8}$ eV, a decrease by seven orders-of-magnitude. In addition, the beam's effective transverse temperature $T_\perp$ and emittance are subject to increase due to nonlinearities in applied and self-field forces, nonstationary beam profiles, and mismatches, which may produce negligible changes in the parallel temperature. This simultaneous cooling in the parallel direction and heating in the transverse direction can provide the free energy to drive collective instabilities and cause a further deterioration in beam quality through the instability mechanism described in this paper.

To briefly summarize the assumptions and macroscopic

warm-fluid model, the present analysis considers an intense non-neutral beam consisting of charged particles with charge q and rest mass m propagating in the z-direction with average axial velocity $V_b=$ const., and characteristic directed kinetic energy $(\gamma_b-1)mc^2$ in the laboratory frame. Here, $\gamma_b=(1-V_b^2/c^2)^{-1/2}$ is the relativistic mass factor, c is the speed of light *in vacuo*, and a perfectly conducting cylindrical wall is located at radius $r=r_w$, where $r=(x^2+y^2)^{1/2}$ is the radial distance from the beam axis. The characteristic beam radius is denoted by r_b, and it is assumed that the particle motion in the beam frame is nonrelativistic. Transverse confinement of the beam particles is provided by applied magnetic or electric focusing fields, and in the *smooth-focusing* approximation we model the applied transverse focusing force on a beam particle by $\mathbf{F}_{\rm foc}=-\gamma_b m\omega_{\beta\perp}^2(x\hat{\mathbf{e}}_x+y\hat{\mathbf{e}}_y)$, where $\omega_{\beta\perp}=$ const. is the effective betatron frequency for the transverse oscillations, and (x,y) is the transverse displacement from the beam axis. Following Lund and Davidson,[50] by taking appropriate momentum moments of the nonlinear Vlasov equation for the beam distribution function $f(\mathbf{x},\mathbf{p},t)$ in the six-dimensional phase space $(\mathbf{x},\mathbf{p})$, we obtain an interconnected chain of macroscopic fluid equations advancing the particle density $n(\mathbf{x},t)$, the average flow velocity $\mathbf{V}(\mathbf{x},t)=V_z(\mathbf{x},t)\hat{\mathbf{e}}_z+\mathbf{V}_\perp(\mathbf{x},t)$, the pressure tensor $\mathbf{P}(\mathbf{x},t)$, the heat-flow tensor $\mathbf{Q}(\mathbf{x},t)$, etc. In the present analysis, we adopt a model[41] in which the heat-flow contribution, proportional to $(\partial/\partial\mathbf{x})\cdot\mathbf{Q}(\mathbf{x},t)$, is neglected in the dynamical equation advancing the pressure tensor $\mathbf{P}(\mathbf{x},t)$, thereby leading to a closed system of macroscopic fluid-Maxwell equations describing beam equilibrium and stability properties. In addition, the pressure tensor $\mathbf{P}(\mathbf{x},t)$ is assumed to be isotropic in the plane perpendicular to the beam propagation direction (the z-direction), i.e., $\mathbf{P}(\mathbf{x},t)=P_\perp(\mathbf{x},t)(\hat{\mathbf{e}}_x\hat{\mathbf{e}}_x+\hat{\mathbf{e}}_y\hat{\mathbf{e}}_y)+P_\parallel(\mathbf{x},t)\hat{\mathbf{e}}_z\hat{\mathbf{e}}_z$, where $P_\perp(\mathbf{x},t)$ and $P_\parallel(\mathbf{x},t)$ are scalar pressures. Finally, under axisymmetric equilibrium conditions with $\partial/\partial\theta=0$, $\partial/\partial t=0$, and $\partial/\partial=0$, the warm fluid-Maxwell equations support a broad class of solutions for the equilibrium density and pressure profiles $n^0(r)$, $P_\perp^0(r)$, and $P_\parallel^0(r)$. In the present anaysis, we limit the detailed investigations of stability behavior for small-amplitude perturbations to the class of so-called *waterbag* equilibria[24,27,50] in which $P_\perp^0(r)=$ const.$[n^0(r)]^2$ and $P_\parallel^0(r)=$ const.$[n^0(r)]$. The stability analysis allows for general pressure anisotropy, permitting a detailed investigation of anisotropy-driven instabilities[37–39] when $P_\perp^0>P_\parallel^0$.

This paper is organized as follows. Following a discussion of the macroscopic warm-fluid model and the waterbag equilibrium in Sec. II, we linearize the macroscopic fluid equations for small-amplitude perturbations in Sec. III, and derive a single eigenvalue equation for the perturbed electrostatic potential $\delta\phi(\mathbf{x},t)$, allowing for arbitrary anisotropy in the perpendicular and parallel pressures, $P_\perp^0(r)$ and $P_\parallel^0(r)$. Detailed stability properties are calculated numerically in Sec. IV for the case of extreme anisotropy with $P_\parallel^0(r)=0$ and $P_\perp^0(r)\neq 0$, assuming axisymmetric wave perturbations $(\partial/\partial\theta=0)$ of the form $\delta\phi(\mathbf{x},t)=\delta\hat{\phi}(r)\exp(ik_z z-i\omega t)$, where k_z is the axial wavenumber, and $Im\,\omega>0$ corresponds to instability (temporal growth). For $k_z=0$, the analysis of the eigenvalue equation leads to a discrete spectrum $\{\omega_n\}$ of stable oscillations with $Im\,\omega_n=0$, where n is the radial mode number (Sec. IV B). On the other hand, for sufficiently large values of $k_z r_b$, where r_b is the beam radius, the analysis of the eigenvalue equation leads to an anisotropy-driven instability $(Im\,\omega>0)$ provided the normalized Debye length $(\Gamma_D=\lambda_{D\perp}/r_b)$ is sufficiently large and the normalized beam intensity $(s_b=\hat{\omega}_{pb}^2/2\gamma_b^2\omega_{\beta\perp}^2)$ is sufficiently below the space-charge limit (Sec. IV C). Depending on system parameters, the growth rate can be a substantial fraction of the focusing frequency $\omega_{\beta\perp}$ of the applied field.

II. ASSUMPTIONS AND THEORETICAL MODEL

In this section, we summarize the assumptions and macroscopic warm-fluid model used in the present equilibrium and stability analysis (Sec. II A), and describe properties of the warm-fluid waterbag equilibrium (Sec. II B). The electrostatic eigenvalue equation describing stability behavior for small-amplitude perturbations about equilibrium is then derived in Sec. III, and detailed stability properties are calculated in Sec. IV.

A. Assumptions and macroscopic warm-fluid model

The present analysis considers an intense non-neutral beam consisting of charged particles with charge q and rest mass m propagating in the z-direction with average axial velocity $V_b=$ const., and characteristic directed kinetic energy $(\gamma_b-1)mc^2$ in the laboratory frame. Here, $\gamma_b=(1-V_b^2/c^2)^{-1/2}$ is the relativistic mass factor, c is the speed of light *in vacuo*, and a perfectly conducting cylindrical wall is located at radius $r=r_w$, where $r=(x^2+y^2)^{1/2}$ is the radial distance from the beam axis. The characteristic beam radius is denoted by r_b. It is assumed that $\nu_B/\gamma_b\ll 1$, where $\nu_B=N_b q^2/mc^2$ is Budker's parameter, $N_b=\int dxdy\,n$ is the number of beam particles per unit axial length, and $n(x,y,z,t)$ is the particle number density. It is also assumed that the particle motion in the beam frame is nonrelativistic. Transverse confinement of the beam particles is provided by applied magnetic or electric focusing fields, and in the *smooth-focusing* approximation we model the applied transverse focusing force on a beam particle by

$$\mathbf{F}_{\rm foc}=-\gamma_b m\omega_{\beta\perp}^2(x\hat{\mathbf{e}}_x+y\hat{\mathbf{e}}_y), \tag{1}$$

where $\omega_{\beta\perp}=$ const. is the effective betatron frequency for the transverse oscillations, and (x,y) is the transverse displacement from the beam axis. The transverse focusing force in Eq. (1) is equivalent to the electric force produced by a (hypothetical) uniformly distributed, fixed charge background with charge density $\rho^0=-\gamma_b m\omega_{\beta\perp}^2/2\pi q=$ const., and is often used to model the *average* focusing properties of an alternating-gradient lattice of magnetic or electric quadrupoles.

The present analysis is carried out in the electrostatic approximation, where the self-electric field $\mathbf{E}^s(\mathbf{x},t)$ produced by the beam space charge is

$$\mathbf{E}^s=-\nabla\phi, \tag{2}$$

and the electrostatic potential $\phi(\mathbf{x},t)$ is determined self-consistently from Poisson's equation, $\nabla^2\phi=-4\pi qn(\mathbf{x},t)$, where $n(\mathbf{x},t)$ is the particle number density. In addition, the axial beam current, $qn(\mathbf{x},t)V_z(\mathbf{x},t)$, where $V_z(\mathbf{x},t)$ is the average axial velocity, produces a transverse self-magnetic field, $\mathbf{B}^s(\mathbf{x},t)$, where

$$\mathbf{B}^s=\nabla A_z\times\hat{\mathbf{e}}_z. \tag{3}$$

Here, $A_z(\mathbf{x},t)$ is determined self-consistently in the magnetostatic approximation from Maxwell's equation, $\nabla^2A_z=-(4\pi/c)qnV_z$. In circumstances where the average axial velocity is approximately uniform over the beam cross section with $V_z\simeq V_b=$const., which we assume to be the case, the self-field potentials, $\phi(\mathbf{x},t)$ and $A_z(\mathbf{x},t)$, are related by the familiar expression, $A_z=(V_b/c)\phi$, and Eq. (3) reduces to

$$\mathbf{B}^s=\frac{1}{c}V_b\nabla\phi\times\hat{\mathbf{e}}_z. \tag{4}$$

Denoting the average flow velocity of a beam fluid element by $\mathbf{V}(\mathbf{x},t)=V_z(\mathbf{x},t)\hat{\mathbf{e}}_z+\mathbf{V}_\perp(\mathbf{x},t)$, where $\mathbf{V}_\perp(\mathbf{x},t)=V_x(\mathbf{x},t)\hat{\mathbf{e}}_x+V_y(\mathbf{x},t)\hat{\mathbf{e}}_y$, and making use of Eqs. (3) and (4), the Lorentz force on a beam fluid element due to the self-electric and self-magnetic fields can be expressed as

$$\begin{aligned}\mathbf{F}^s_{\rm Lorentz}&=nq\left(\mathbf{E}^s+\frac{1}{c}\mathbf{V}\times\mathbf{B}^s\right)\\&=-nq\left(1-\frac{V_bV_z}{c^2}\right)\nabla_\perp\phi\\&\quad-nq\left(\frac{\partial\phi}{\partial z}-\frac{V_b}{c^2}\mathbf{V}_\perp\cdot\nabla_\perp\phi\right)\hat{\mathbf{e}}_z,\end{aligned} \tag{5}$$

where $\nabla_\perp=\hat{\mathbf{e}}_x\partial/\partial x+\hat{\mathbf{e}}_y\partial/\partial y$. Approximating $V_z\simeq V_b$ and making use of $|\mathbf{V}_\perp|\ll c$ (nonrelativistic transverse motion), Eq. (5) reduces to the simple expression

$$\mathbf{F}^s_{\rm Lorentz}=-nq\left(\frac{1}{\gamma_b^2}\nabla_\perp\phi+\hat{\mathbf{e}}_z\frac{\partial}{\partial z}\phi\right), \tag{6}$$

where $\gamma_b^{-2}=1-V_b^2/c^2$. Equation (6) shows (as expected) that the net effect of the self-magnetic field $\mathbf{B}^s$ produced by the directed axial motion (generally relativistic) of the beam particles is to *reduce* the perpendicular electrostastic force by the factor $1/\gamma_b^2$.

To describe the dynamics of the intense charged particle beam interacting with the applied focusing field and the self-generated electric and magnetic fields, $\mathbf{E}^s$ and $\mathbf{B}^s$, we make use of the macroscopic warm-fluid model developed by Lund and Davidson,[50] appropriately generalized to the case where the directed axial motion of the beam is allowed to be relativistic. To briefly summarize, by taking appropriate momentum moments of the nonlinear Vlasov equation for the beam distribution function $f(\mathbf{x},\mathbf{p},t)$ in the six-dimensional phase space $(\mathbf{x},\mathbf{p})$, we obtain an interconnected chain of macroscopic fluid equations[41] advancing the particle density $n(\mathbf{x},t)$, the average flow velocity $\mathbf{V}(\mathbf{x},t)=V_z(\mathbf{x},t)\hat{\mathbf{e}}_z+\mathbf{V}_\perp(\mathbf{x},t)$, the pressure tensor $\mathbf{P}(\mathbf{x},t)$, the heat flow tensor $\mathbf{Q}(\mathbf{x},t)$, etc. Following Lund and Davidson,[50] we adopt a model[41] in which the heat-flow contribution, proportional to $(\partial/\partial\mathbf{x})\cdot\mathbf{Q}(\mathbf{x},t)$, is neglected in the dynamical equation advancing the pressure tensor $\mathbf{P}(\mathbf{x},t)$. In addition, we adopt a model[50] in which $\mathbf{P}(\mathbf{x},t)$ is assumed to be isotropic in the plane perpendicular to the beam propagation direction (the z-direction), i.e.,

$$\mathbf{P}(\mathbf{x},t)=P_\perp(\mathbf{x},t)(\hat{\mathbf{e}}_x\hat{\mathbf{e}}_x+\hat{\mathbf{e}}_y\hat{\mathbf{e}}_y)+P_\parallel(\mathbf{x},t)\hat{\mathbf{e}}_z\hat{\mathbf{e}}_z, \tag{7}$$

where $P_\perp(\mathbf{x},t)$ and $P_\parallel(\mathbf{x},t)$ are scalar pressures. In this case, making use of Eqs. (1), (6), and (7), and the assumptions enumerated earlier in this section, the warm fluid-Maxwell equations[50] appropriately generalized to the case of relativistic axial motion are given by the continuity equation for $n(\mathbf{x},t)$,

$$\left(\frac{\partial}{\partial t}+V_z\frac{\partial}{\partial z}+\mathbf{V}_\perp\cdot\frac{\partial}{\partial\mathbf{x}_\perp}\right)n+n\left(\frac{\partial V_z}{\partial z}+\frac{\partial}{\partial\mathbf{x}_\perp}\cdot\mathbf{V}_\perp\right)=-0, \tag{8}$$

the perpendicular force balance equation for $\mathbf{V}_\perp(\mathbf{x},t)$,

$$\begin{aligned}&\gamma_bmn\left(\frac{\partial}{\partial t}+V_z\frac{\partial}{\partial z}+\mathbf{V}_\perp\cdot\frac{\partial}{\partial\mathbf{x}_\perp}\right)\mathbf{V}_\perp+\frac{\partial}{\partial\mathbf{x}_\perp}P_\perp\\&\quad=-nq\frac{1}{\gamma_b^2}\nabla_\perp\phi-\gamma_bmn\omega_{\beta\perp}^2\mathbf{x}_\perp,\end{aligned} \tag{9}$$

the parallel force balance equation for $V_z(\mathbf{x},t)$,

$$\gamma_bmn\left(\frac{\partial}{\partial t}+V_z\frac{\partial}{\partial z}+\mathbf{V}_\perp\cdot\frac{\partial}{\partial\mathbf{x}_\perp}\right)V_z+\frac{\partial}{\partial z}P_\parallel=-nq\frac{\partial\phi}{\partial z}, \tag{10}$$

the equation of state for the perpendicular pressure $P_\perp(\mathbf{x},t)$,

$$\left(\frac{\partial}{\partial t}+V_z\frac{\partial}{\partial z}+\mathbf{V}_\perp\cdot\frac{\partial}{\partial\mathbf{x}_\perp}\right)\left(\frac{P_\perp}{n^2}\right)-\frac{P_\perp}{n^2}\frac{\partial V_z}{\partial z}=0, \tag{11}$$

the equation of state for the parallel pressure $P_\parallel(\mathbf{x},t)$,

$$\left(\frac{\partial}{\partial t}+V_z\frac{\partial}{\partial z}+\mathbf{V}_\perp\cdot\frac{\partial}{\partial\mathbf{x}_\perp}\right)\left(\frac{P_\parallel}{n}\right)+\frac{2P_\parallel}{n}\frac{\partial V_z}{\partial z}=0, \tag{12}$$

and Poisson's equation for the electrostatic potential $\phi(\mathbf{x},t)$,

$$\nabla_\perp^2\phi+\frac{\partial^2}{\partial z^2}\phi=-4\pi qn. \tag{13}$$

Equations (8)–(13) provide a closed macroscopic description of the nonlinear evolution of the beam interacting with the applied focusing field and the self-generated electric and magnetic fields, $\mathbf{E}^s=-\nabla\phi$ and $\mathbf{B}^s=(V_b/c)\nabla\phi\times\hat{\mathbf{e}}_z$. In obtaining Eqs. (8)–(13), it has been assumed that the fluid motions in the beam frame are nonrelativistic, i.e.,

$$\mathbf{V}_\perp^2/c^2,\ (V_z-V_b)^2/c^2,\ P_\perp/\gamma_bnmc^2,\ P_\parallel/\gamma_bnmc^2\ll1. \tag{14}$$

Equations (8)–(13) can be used to investigate detailed macroscopic equilibrium and stability properties for perturbations about a wide range of beam equilibria ranging from a warm-fluid thermal equilibrium with diffuse radial density profile, to a warm-fluid Kapchinskij–Vladimirskij (KV) equilibrium with step-function density profile,[50] to a warm-fluid waterbag equilibrium.[50] For example, assuming $\partial/\partial z=0$, Lund and Davidson have investigated[50] stable electro-

static oscillations for perturbations about a warm-fluid KV equilibrium. In the present analysis, allowing for a pressure anisotropy with $P_\perp \neq P_\parallel$ and perturbations with $\partial/\partial z \neq 0$, in Secs. III and IV we examine detailed stability properties for perturbations about a warm-fluid waterbag equilibrium.[24,27,50] We conclude Sec. II with a brief summary of equilibrium properties for a warm-fluid waterbag equilibrium in which the equilibrium perpendicular pressure is assumed to have the double adiabatic form $P_\perp^0(r) = \text{const.}[n^0(r)]^2$.

B. Warm-fluid waterbag equilibrium

Under steady-state (equilibrium) conditions with $\partial/\partial t = 0$, we assume a matched, axisymmetric beam in which all equilibrium profiles (denoted with a superscript zero), $n^0(\mathbf{x})$, $\phi^0(\mathbf{x})$, $\mathbf{V}_\perp^0(\mathbf{x})$, $V_z^0(\mathbf{x})$, $P_\perp^0(\mathbf{x})$ and $P_\parallel^0(\mathbf{x})$, satisfy

$$\frac{\partial}{\partial \theta} = 0 = \frac{\partial}{\partial z}, \tag{15}$$

and depend only on the radial distance $r = (x^2 + y^2)^{1/2}$ from the beam axis. In equilibrium, it is further assumed that there is no perpendicular motion of the beam and that the axial flow velocity is uniform over the beam cross section, i.e.,

$$\mathbf{V}_\perp^0 = 0, \quad V_z^0 = V_b = \text{const.} \tag{16}$$

For a warm-fluid waterbag equilibrium,[24,27,50] we assume that the perpendicular and parallel pressures are of the form

$$P_\perp^0(r) = \frac{\hat{T}_\perp}{\hat{n}}[n^0(r)]^2, \quad P_\parallel^0(r) = \hat{T}_\parallel n^0(r), \tag{17}$$

where $n^0(r)$ is the equilibrium density profile. In Eq. (17), $\hat{n} = n^0(r=0) = \text{const.}$ is the on-axis density, and the constants $\hat{T}_\perp$ and $\hat{T}_\parallel$ are the perpendicular temperature and parallel temperature, respectively, at $r = 0$, expressed in energy units. From Eq. (17), we note that the effective temperature profiles, $T_\perp^0(r) = P_\perp^0(r)/n^0(r)$ and $T_\parallel^0(r) = P_\parallel^0(r)/n^0(r)$, are given by $T_\perp^0(r) = \hat{T}_\perp n^0(r)/\hat{n}$ and $T_\parallel^0(r) = \hat{T}_\parallel = \text{const.}$ That is, $T_\perp^0(r)$ has the same radial shape as the density profile $n^0(r)$, whereas $T_\parallel^0(r)$ is uniform (isothermal) over the beam cross section.

Making use of $\partial/\partial t = 0$ and Eqs. (15)–(17), it is readily shown that Eqs. (8), (10), (11), and (12) are automatically satisfied, and that Eqs. (9) and (13) reduce exactly to

$$\frac{2\hat{T}_\perp}{\hat{n}} n^0 \frac{\partial}{\partial r} n^0 = -n^0 \left(\frac{q}{\gamma_b^2} \frac{\partial \phi^0}{\partial r} + \gamma_b m \omega_{\beta\perp}^2 r \right), \tag{18}$$

$$\frac{1}{r} \frac{\partial}{\partial r} r \frac{\partial}{\partial r} \phi^0 = -4\pi q n^0, \tag{19}$$

where $n^0(r)$ and $\phi^0(r)$ are the equilibrium density and potential profiles. Equations (18) and (19) can be solved exactly for the equilibrium density profile $n^0(r)$. We introduce the effective perpendicular Debye length $\lambda_{D\perp}$ and self-field intensity parameter s_b defined by

$$\lambda_{D\perp}^2 = \frac{2\hat{T}_\perp \gamma_b^2}{4\pi q^2 \hat{n}}, \quad s_b = \frac{\hat{\omega}_{pb}^2}{2\gamma_b^2 \omega_{\beta\perp}^2}, \tag{20}$$

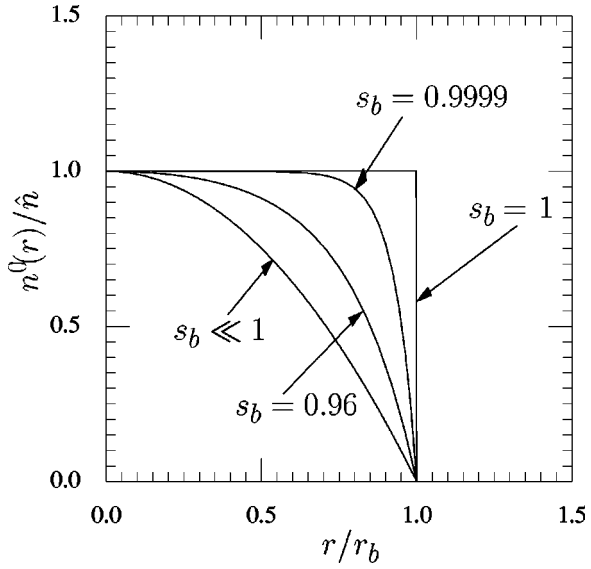

FIG. 1. Plot of the normalized density $n^0(r)/\hat{n}$ versus r/r_b calculated from Eqs. (21) and (22) for several values of the normalized beam intensity $s_b = \hat{\omega}_{pb}^2/2\gamma_b^2\omega_{\beta\perp}^2$.

where $\hat{\omega}_{pb}^2 = 4\pi\hat{n}q^2/\gamma_b m$ is the on-axis plasma frequency-squared. Without presenting algebraic details, the exact solution to Eqs. (18) and (19) is given by

$$n^0(r) = \begin{cases} \hat{n}\dfrac{I_0(r_b/\lambda_{D\perp}) - I_0(r/\lambda_{D\perp})}{I_0(r_b/\lambda_{D\perp}) - 1}, & 0 \leqslant r < r_b, \\ 0, & r_b < r \leqslant r_w, \end{cases} \tag{21}$$

where r_b is the outer radius of the beam, and r_w is the conducting wall radius. In terms of $\lambda_{D\perp}$ and $s_b = \hat{\omega}_{pb}^2/2\gamma_b^2\omega_{\beta\perp}^2$, the beam radius r_b in Eq. (21) is determined self-consistently from

$$I_0(r_b/\lambda_{d\perp}) = \frac{1}{1 - \hat{\omega}_{pb}^2/2\gamma_b^2\omega_{\beta\perp}^2}. \tag{22}$$

In Eqs. (21) and (22), $I_0(x)$ is the modified Bessel function of the first kind of order zero.

For the equilibrium density profile $n^0(r)$ specified by Eq. (21), we note that the profiles for $P_\perp^0(r)$, $P_\parallel^0(r)$, and $\phi^0(r)$ are fully determined from Eqs. (17) and (19). In addition, from Eq. (21), the density profile decreases monotonically from the on-axis value $n^0(r=0) = \hat{n}$ at $r = 0$, to $n^0(r = r_b) = 0$ at the beam edge ($r = r_b$). At low beam intensities with $s_b = \hat{\omega}_{pb}^2/2\gamma_b^2\omega_{\beta\perp}^2 \ll 1$, it follows from Eq. (22) that $r_b < \lambda_{D\perp}$, corresponding to an emittance-dominated beam with near-parabolic density profile, $n^0(r) = \hat{n}(1 - r^2/r_b^2)$, over the beam cross section. On the other hand, for $s_b = \hat{\omega}_{pb}^2/2\gamma_b^2\omega_{\beta\perp}^2 \to 1 - \epsilon$, with $\epsilon \to 0_+$, it follows from Eq. (21) that $r_b \gg \lambda_{D\perp}$ and that $n^0(r)$ approaches the step-function density profile characteristic of space-charge-dominated beams with very low transverse emittance. These properties are illustrated in Figs. 1 and 2. In Fig. 1, the normalized density profile $n^0(r)/\hat{n}$ calculated from Eq. (21) is plotted versus r/r_b for several values of the dimensionless

intensity parameter $s_b=\hat{\omega}_{pb}^2/2\gamma_b^2\omega_{\beta\perp}^2$ over the interval $0<s_b<1$. On the other hand, Fig. 2 shows a universal plot of the normalized Debye length $\lambda_{D\perp}/r_b$ versus $s_b=\hat{\omega}_{pb}^2/2\gamma_b^2\omega_{\beta\perp}^2$ for values of the beam intensity parameter in the interval $0<s_b<1$.

III. EIGENVALUE EQUATION FOR SMALL-AMPLITUDE PERTURBATIONS

In this section, we linearize the macroscopic fluid equations (8)–(13) for small-amplitude perturbations about the warm-fluid waterbag equilibrium described by Eqs. (15)–(22) (Sec. III A). The resulting linearized equations are then expressed as a single eigenvalue equation for the perturbed electrostatic potential $\delta\phi(\mathbf{x},t)$, allowing for arbitrary anisotropy in the perpendicular and parallel pressures, $P_\perp^0(r)$ and $P_\parallel^0(r)$ (Sec. III B).

A. Linearized warm-fluid-Maxwell equations

We now express

$$\begin{aligned} &n(\mathbf{x},t)=n^0(r)+\delta n(\mathbf{x},t), \quad \mathbf{V}_\perp(\mathbf{x},t)=\delta\mathbf{V}_\perp(\mathbf{x},t),\\ &V_z(\mathbf{x},t)=V_b+\delta V_z(\mathbf{x},t), \quad P_\perp(\mathbf{x},t)=P_\perp^0(r)+\delta P_\perp(\mathbf{x},t),\\ &P_\parallel(\mathbf{x},t)=P_\parallel^0(r)+\delta P_\parallel(\mathbf{x},t), \quad \phi(\mathbf{x},t)=\phi^0(r)+\delta\phi(\mathbf{x},t), \end{aligned} \tag{23}$$

and linearize Eqs. (8)–(13) for small-amplitude perturbations about the warm-fluid waterbag equilibrium described by Eqs. (15)–(22). Because

$$\begin{aligned} &-\delta n\left(\frac{q}{\gamma_b^2}\nabla_\perp\phi^0+\gamma_b m\omega_{\beta\perp}^2\mathbf{x}_\perp\right)=\delta n\frac{1}{n^0}\frac{\partial}{\partial\mathbf{x}_\perp}P_\perp^0,\\ &\delta\mathbf{V}_\perp\cdot\frac{\partial}{\partial\mathbf{x}_\perp}\left(\frac{P_\perp^0}{n^{0^2}}\right)=0, \quad \delta\mathbf{V}_\perp\cdot\frac{\partial}{\partial\mathbf{x}_\perp}\left(\frac{P_\parallel^0}{n^0}\right)=0, \end{aligned} \tag{24}$$

follow directly from Eqs. (17) and (18), the linearized equations for δn, $\delta\mathbf{V}_\perp$, δV_z, $\delta P_\perp$, $\delta P_\parallel$ and $\delta\phi$ obtained from Eqs. (8)–(13) are readily simplified. We obtain after some straightforward algebra

$$\left(\frac{\partial}{\partial t}+V_b\frac{\partial}{\partial z}\right)\delta n+\frac{\partial}{\partial\mathbf{x}_\perp}\cdot(n^0\delta\mathbf{V}_\perp)+n^0\frac{\partial}{\partial z}\delta V_z=0, \tag{25}$$

$$\gamma_b m n^0\left(\frac{\partial}{\partial t}+V_b\frac{\partial}{\partial z}\right)\delta\mathbf{V}_\perp=-\left(\frac{\partial}{\partial\mathbf{x}_\perp}\delta P_\perp-\frac{\delta n}{n^0}\frac{\partial}{\partial\mathbf{x}_\perp}P_\perp^0+\frac{n^0 q}{\gamma_b^2}\frac{\partial}{\partial\mathbf{x}_\perp}\delta\phi\right), \tag{26}$$

$$\gamma_b m n^0\left(\frac{\partial}{\partial t}+V_b\frac{\partial}{\partial z}\right)\delta V_z=-\left(\frac{\partial}{\partial z}\delta P_\parallel+n^0 q\frac{\partial}{\partial z}\delta\phi\right), \tag{27}$$

where $\delta P_\perp$, $\delta P_\parallel$, and $\delta\phi$ evolve according to

$$\left(\frac{\partial}{\partial t}+V_b\frac{\partial}{\partial z}\right)\left(\delta P_\perp-\frac{2\delta n}{n^0}P_\perp^0\right)-P_\perp^0\frac{\partial}{\partial z}\delta V_z=0, \tag{28}$$

$$\left(\frac{\partial}{\partial t}+V_b\frac{\partial}{\partial z}\right)\left(\delta P_\parallel-\frac{\delta n}{n^0}P_\parallel^0\right)+2P_\parallel^0\frac{\partial}{\partial z}\delta V_z=0, \tag{29}$$

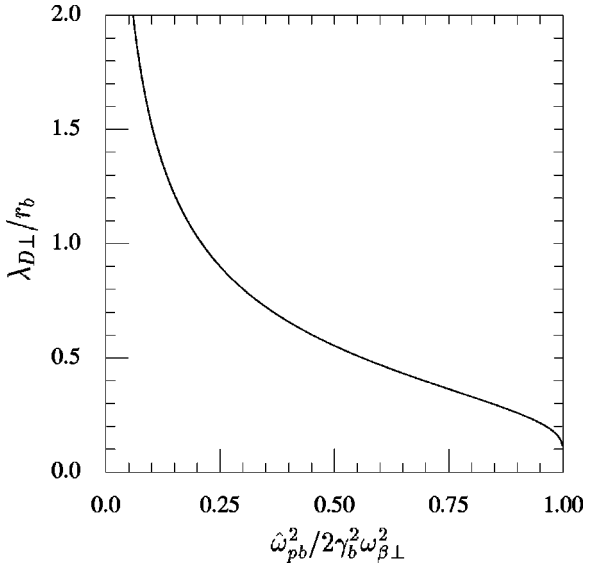

FIG. 2. Plot of the normalized Debye length $\lambda_{D\perp}/r_b$ versus $s_b=\hat{\omega}_{pb}^2/2\gamma_b^2\omega_{\beta\perp}^2$ calculated numerically from Eq. (22) for values of the normalized beam intensity in the interval $0<s_b<1$.

$$\nabla_\perp^2\delta\phi+\frac{\partial^2}{\partial z^2}\delta\phi=-4\pi q\,\delta n. \tag{30}$$

Here, the equilibrium profiles for $n^0(r)$, $P_\perp^0(r)$, and $P_\parallel^0(r)$ are specified by Eqs. (17) and (21). Equations (25)–(30) can be further simplified by operating on Eqs. (25), (28), and (29) with $(\partial/\partial t+V_b\partial/\partial z)$, and making use of Eqs. (26) and (27) to eliminate $(\partial/\partial t+V_b\partial/\partial z)(n^0\delta\mathbf{V}_\perp)$ and $(\partial/\partial t+V_b\partial/\partial z)(n^0\delta V_z)$. This gives

$$\begin{aligned} &\left(\frac{\partial}{\partial t}+V_b\frac{\partial}{\partial z}\right)^2(4\pi q\,\delta n)-\frac{4\pi q}{\gamma_b m}\frac{\partial^2}{\partial z^2}(\delta P_\parallel+n^0 q\,\delta\phi)\\ &\quad-\frac{4\pi q}{\gamma_b m}\frac{\partial}{\partial\mathbf{x}_\perp}\cdot\left(\frac{\partial}{\partial\mathbf{x}_\perp}\delta P_\perp-\frac{\delta n}{n^0}\frac{\partial}{\partial\mathbf{x}_\perp}P_\perp^0+\frac{n^0 q}{\gamma_b^2}\frac{\partial}{\partial\mathbf{x}_\perp}\delta\phi\right)\\ &\quad=0, \end{aligned} \tag{31}$$

$$\begin{aligned} &\left(\frac{\partial}{\partial t}+V_b\frac{\partial}{\partial z}\right)^2\left(\delta P_\perp-\frac{2\delta n}{n^0}P_\perp^0\right)+\frac{P_\perp^0}{\gamma_b m n^0}\frac{\partial^2}{\partial z^2}(\delta P_\parallel\\ &\quad+n^0 q\,\delta\phi)=0, \end{aligned} \tag{32}$$

$$\begin{aligned} &\left[\left(\frac{\partial}{\partial t}+V_b\frac{\partial}{\partial z}\right)^2-\frac{2P_\parallel^0}{\gamma_b m n^0}\frac{\partial^2}{\partial z^2}\right](\delta P_\parallel+n^0 q\,\delta\phi)\\ &\quad-\left(\frac{\partial}{\partial t}+V_b\frac{\partial}{\partial z}\right)^2\left(\frac{\delta n}{n^0}P_\parallel^0+n^0 q\,\delta\phi\right)=0. \end{aligned} \tag{33}$$

We now make use of $P_\perp^0(r)=(\hat{T}_\perp/\hat{n})[n^0(r)]^2$ and $P_\parallel^0(r)=n^0(r)\hat{T}_\parallel$, where $\hat{T}_\perp$ and $\hat{T}_\parallel$ are positive constants [Eq. (17)], and introduce the definitions [see also Eq. (20)]

$$\omega_{pb}^2(r)=\frac{4\pi n^0(r)q^2}{\gamma_b m}, \quad v_{TZ}^2=\frac{2\hat{T}_\parallel}{\gamma_b m}, \quad \lambda_{D\perp}^2=\frac{2\hat{T}_\perp\gamma_b^2}{4\pi\hat{n}q^2}. \tag{34}$$

Here, $\omega_{pb}^2(r)$ is the local relativistic plasma frequency-squared, and the constants v_{TZ} and $\lambda_{D\perp}$ are the effective

axial thermal speed and *perpendicular Debye length*, respectively. Making use of Eqs. (17) and (34), it is readily shown that

$$\frac{2P_{\parallel}^{0}(r)}{\gamma_b m n^{0}(r)} = v_{TZ}^{2}, \quad \frac{P_{\perp}^{0}(r)}{\gamma_b m n^{0}(r)} = \frac{1}{2\gamma_b^{2}}\lambda_{D\perp}^{2}\omega_{pb}^{2}(r),$$

$$\frac{1}{\gamma_b m n^{0}(r)}\frac{\partial}{\partial \mathbf{x}_\perp}P_{\perp}^{0}(r) = \frac{1}{\gamma_b^{2}}\lambda_{D\perp}^{2}\frac{\partial}{\partial \mathbf{x}_\perp}\omega_{pb}^{2}(r). \tag{35}$$

Making use of Eqs. (34) and (35), it is straightforward to show that Eqs. (31)–(33) can be expressed in the equivalent form

$$\left(\frac{\partial}{\partial t}+V_b\frac{\partial}{\partial z}\right)^{2}(4\pi q\,\delta n) - \frac{\partial^{2}}{\partial z^{2}}\left[\left(\frac{4\pi q}{\gamma_b m}\delta P_{\parallel}\right)+\omega_{pb}^{2}(r)\,\delta\phi\right]$$
$$-\frac{\partial}{\partial \mathbf{x}_\perp}\cdot\left[\frac{\partial}{\partial \mathbf{x}_\perp}\left(\frac{4\pi q}{\gamma_b m}\delta P_{\perp}\right)-(4\pi q\,\delta n)\frac{\lambda_{D\perp}^{2}}{\gamma_b^{2}}\frac{\partial}{\partial \mathbf{x}_\perp}\omega_{pb}^{2}(r)\right.$$
$$\left.+\frac{1}{\gamma_b^{2}}\omega_{pb}^{2}(r)\frac{\partial}{\partial \mathbf{x}_\perp}\delta\phi\right]=0, \tag{36}$$

$$\left(\frac{\partial}{\partial t}+V_b\frac{\partial}{\partial z}\right)^{2}\left[\left(\frac{4\pi q}{\gamma_b m}\delta P_{\perp}\right)-(4\pi q\,\delta n)\frac{\lambda_{D\perp}^{2}}{\gamma_b^{2}}\omega_{pb}^{2}(r)\right]$$
$$+\frac{1}{2}\frac{\lambda_{D\perp}^{2}}{\gamma_b^{2}}\omega_{pb}^{2}(r)\frac{\partial^{2}}{\partial z^{2}}\left[\left(\frac{4\pi q}{\gamma_b m}\delta P_{\parallel}\right)+\omega_{pb}^{2}(r)\,\delta\phi\right]=0, \tag{37}$$

$$\left[\left(\frac{\partial}{\partial t}+V_b\frac{\partial}{\partial z}\right)^{2}-v_{TZ}^{2}\frac{\partial^{2}}{\partial z^{2}}\right]\left[\left(\frac{4\pi q}{\gamma_b m}\delta P_{\parallel}\right)+\omega_{pb}^{2}(r)\,\delta\phi\right]$$
$$-\left(\frac{\partial}{\partial t}+V_b\frac{\partial}{\partial z}\right)^{2}\left[\frac{1}{2}(4\pi q\,\delta n)v_{TZ}^{2}+\omega_{pb}^{2}(r)\,\delta\phi\right]=0. \tag{38}$$

Keeping in mind that $\delta n(\mathbf{x},t)$ and $\delta\phi(\mathbf{x},t)$ are related by Poisson's equation, $4\pi q\,\delta n = -(\nabla_\perp\delta\phi+\partial^{2}\delta\phi/\partial z^{2})$ [Eq. (30)], it is clear that Eqs. (36)–(38) represent three coupled equations describing the evolution of $\delta\phi(\mathbf{x},t)$, $\delta P_{\parallel}(\mathbf{x},t)$, and $\delta P_{\perp}(\mathbf{x},t)$ in the linearization approximation. Furthermore, because $\lambda_{D\perp}^{2}\propto\hat{T}_\perp$ and $v_{TZ}^{2}\propto\hat{T}_\parallel$, it is also evident that Eqs. (36)–(38) incorporate the effects of an equilibrium pressure anisotropy on stability behavior. Equations (36)–(38) can be simplified in various limiting regimes. For example, if the beam is cold in the axial direction with $\hat{T}_\parallel=0$ ($P_{\parallel}^{0}=0$), it follows directly from Eq. (38) that $(\partial/\partial t+V_b\partial/\partial z)^{2}\delta P_{\parallel}(\mathbf{x},t)=0$. Therefore, if $\delta P_{\parallel}$ is equal to zero initially, then $\delta P_{\parallel}$ remains equal to zero at subsequent times in the linearization approximation.

B. Eigenvalue equation

Equations (30), (36), (37), and (38) are readily combined into a single eigenvalue equation for the perturbed electrostatic potential $\delta\phi$ and the complex oscillation frequency ω. Using a normal-mode approach, we express all perturbed quantities $\delta\phi(\mathbf{x},t)$, $\delta P_{\perp}(\mathbf{x},t)$, $\delta P_{\parallel}(\mathbf{x},t)$, and $\delta n(\mathbf{x},t)$ as

$$\delta\psi(\mathbf{x},t)=\delta\hat{\psi}(\mathbf{x}_\perp)\exp(ik_z z-i\omega t). \tag{39}$$

Here, $\delta\hat{\psi}(\mathbf{x}_\perp)$ is the perturbation amplitude, k_z is the axial wavenumber of the perturbation, and ω is the complex oscillation frequency, with $Im\,\omega>0$ corresponding to instability (temporal growth). We further introduced the Doppler-shifted oscillation frequency Ω defined by

$$\Omega=\omega-k_z V_b. \tag{40}$$

Substituting Eq. (39) into Eq. (38) and making use of Poisson's equation,

$$\nabla_\perp^{2}\delta\hat{\phi}(\mathbf{x}_\perp)-k_z^{2}\delta\hat{\phi}(\mathbf{x}_\perp)=-4\pi q\,\delta\hat{n}(\mathbf{x}_\perp), \tag{41}$$

we readily obtain for $\delta\hat{P}_{\parallel}(\mathbf{x}_\perp)$,

$$\frac{4\pi q}{\gamma_b m}\delta\hat{P}_{\parallel}+\omega_{pb}^{2}(r)\,\delta\hat{\phi} = \frac{\Omega^{2}}{\Omega^{2}-k_z^{2}v_{TZ}^{2}}\left[-\frac{1}{2}v_{TZ}^{2}(\nabla_\perp^{2}\delta\hat{\phi}-k_z^{2}\delta\hat{\phi})+\omega_{pb}^{2}(r)\,\delta\hat{\phi}\right]. \tag{42}$$

Similarly, making use of Eq. (37) and (42), gives for $\delta\hat{P}_{\perp}(\mathbf{x}_\perp)$,

$$\frac{4\pi q}{\gamma_b m}\delta\hat{P}_{\perp} = -\lambda_{D\perp}^{2}\frac{\omega_{pb}^{2}(r)}{\gamma_b^{2}}(\nabla_\perp^{2}\delta\hat{\phi}-k_z^{2}\delta\hat{\phi}) - \frac{1}{2}k_z^{2}\lambda_{D\perp}^{2}\frac{\omega_{pb}^{2}(r)/\gamma_b^{2}}{\Omega^{2}-k_z^{2}v_{TZ}^{2}}\left[-\frac{1}{2}v_{TZ}^{2}(\nabla_\perp^{2}\delta\hat{\phi}-k_z^{2}\delta\hat{\phi})+\omega_{pb}^{2}(r)\,\delta\hat{\phi}\right]. \tag{43}$$

Equations (42) and (43) constitute closed expressions for the pressure perturbations, $\delta\hat{P}_{\parallel}(\mathbf{x}_\perp)$ and $\delta\hat{P}_{\perp}(\mathbf{x})$, directly in terms of the potential amplitude $\delta\hat{\phi}(\mathbf{x})$, the equilibrium density profile $\omega_{pb}^{2}(r)$, the Doppler-shifted oscillation frequency $\Omega=\omega-k_z V_b$, and the constant parameters $\lambda_{D\perp}^{2}$ and v_{TZ}^{2}. As noted earlier, for the special case where $\hat{T}_\parallel=0$, Eq. (42) gives

$$\delta\hat{P}_{\parallel}=0, \quad \text{for } v_{TZ}^{2}=0. \tag{44}$$

We now make use of Eqs. (39) and (40) and substitute Eqs. (41)–(43) into Eq. (36). This results in a single eigenvalue equation for the potential eigenfunction $\delta\hat{\phi}(\mathbf{x}_\perp)$ and the complex oscillation frequency $\Omega=\omega-k_z V_b$. After some algebraic manipulation and rearrangement of terms, we obtain

$$\frac{\partial}{\partial \mathbf{x}_\perp}\cdot\left\{\left[\Omega^{2}-\frac{\omega_{pb}^{2}(r)}{\gamma_b^{2}}(1+k_z^{2}\lambda_{D\perp}^{2})-\frac{\frac{1}{2}k_z^{2}v_{TZ}^{2}\Omega^{2}}{\Omega^{2}-k_z^{2}v_{TZ}^{2}}\right]\frac{\partial}{\partial \mathbf{x}_\perp}\delta\hat{\phi}\right.$$
$$+\lambda_{D\perp}^{2}\frac{\omega_{pb}^{2}(r)}{\gamma_b^{2}}\frac{\partial}{\partial \mathbf{x}_\perp}\nabla_\perp^{2}\delta\hat{\phi}+\frac{1}{2}k_z^{2}\lambda_{D\perp}^{2}\frac{\partial}{\partial \mathbf{x}_\perp}\left[\frac{\omega_{pb}^{2}(r)/\gamma_b^{2}}{\Omega^{2}-k_z^{2}v_{TZ}^{2}}\right.$$
$$\left.\left.\times\left(\left[\omega_{pb}^{2}(r)+\frac{1}{2}k_z^{2}v_{TZ}^{2}\right]\delta\hat{\phi}-\frac{1}{2}v_{TZ}^{2}\nabla_\perp^{2}\delta\hat{\phi}\right)\right]\right\}$$

$$-k_z^2\left\{\Omega^2-\frac{\omega_{pb}^2(r)\Omega^2}{\Omega^2-k_z^2v_{TZ}^2}-\frac{\frac{1}{2}k_z^2v_{TZ}^2\Omega^2}{\Omega^2-k_z^2v_{TZ}^2}\right\}\delta\hat{\phi}=0. \tag{45}$$

Equation (45) is the final eigenvalue equation for the potential eigenfunction $\delta\hat{\phi}(\mathbf{x}_\perp)$ and the eigenfrequency $\Omega=\omega-k_zV_b$. Equation (45) has been derived from Eqs. (25)–(30) for small-amplitude perturbations about the warm-fluid waterbag equilibrium described by Eqs. (17) and (21), and can be used to investigate detailed stability properties over a wide range of values of the normalized beam intensity $s_b=\hat{\omega}_{pb}^2/2\gamma_b^2\omega_{\beta\perp}^2$, and temperature anisotropy $\hat{T}_\perp-\hat{T}_\parallel$. Anisotropy-driven instabilities are expected to be the strongest in the case of strong temperature anisotropy $\hat{T}_\perp\gg\hat{T}_\parallel$. In circumstances where the beam ions are cold in the propagation direction, the eigenvalue equation (45) simplifies considerably. Setting $\hat{T}_\parallel=0$ $(v_{TZ}^2=0)$ in Eq. (45), we obtain

$$\begin{aligned}\frac{\partial}{\partial\mathbf{x}_\perp}\cdot\Bigg\{&\left[\Omega^2-\frac{\omega_{pb}^2(r)}{\gamma_b^2}(1+k_z^2\lambda_{D\perp}^2)\right]\frac{\partial}{\partial\mathbf{x}_\perp}\delta\hat{\phi}\\&+\lambda_{D\perp}^2\frac{\omega_{pb}^2(r)}{\gamma_b^2}\frac{\partial}{\partial\mathbf{x}_\perp}\nabla_\perp^2\delta\hat{\phi}\\&+\frac{1}{2}k_z^2\lambda_{D\perp}^2\frac{\partial}{\partial\mathbf{x}_\perp}\left(\frac{\omega_{pb}^4(r)/\gamma_b^2}{\Omega^2}\delta\hat{\phi}\right)\Bigg\}\\&-k_z^2[\Omega^2-\omega_{pb}^2(r)]\delta\hat{\phi}=0.\end{aligned} \tag{46}$$

Introducing cylindrical polar coordinates (r,θ), where $x=r\cos\theta$ and $y=r\sin\theta$, we represent $\delta\hat{\phi}(\mathbf{x}_\perp)=\delta\hat{\phi}(r,\theta)$. The eigenvalue equations (45) or (46) are to be solved for $\delta\hat{\phi}(r,\theta)$ and Ω subject to the requirements that $\delta\hat{\phi}(r,\theta)$ be regular at the origin $(r=0)$, and that

$$\delta\hat{\phi}(r=r_w,\theta)=0. \tag{47}$$

The boundary condition in Eq. (47) of course assures that the perturbed tangential electric field components vanish at the perfectly conducting wall, i.e., $[\delta\hat{E}_\theta]_{r=r_w}=-[r^{-1}\partial\delta\hat{\phi}/\partial\theta]_{r=r_w}=0$ and $[\delta\hat{E}_z]_{r=r_w}=-ik_z[\delta\hat{\phi}]_{r=r_w}=0$.

IV. STABILITY ANALYSIS

A. Eigenvalue equation for $\hat{T}_\parallel=0$ and $(\partial/\partial\theta)\delta\hat{\phi}=0$

As noted earlier, for equilibrium density profile $n^0(r)$ specified by Eq. (21), the eigenvalue equation (45) can be used to investigate detailed stability behavior over a wide range of values of normalized beam intensity $s_b=\hat{\omega}_{pb}^2/2\gamma_b^2\omega_{\beta\perp}^2$, and temperature anisotropy $\hat{T}_\perp-\hat{T}_\parallel$. Since this is the first theoretical study of macroscopic stability properties for perturbations about a warm-fluid waterbag equilibrium, the present analysis is restricted to the case of extreme temperature anisotropy with $\hat{T}_\parallel=0$, assuming azimuthally symmetric perturbations with $(\partial/\partial\theta)\delta\hat{\phi}(r,\theta)=0$. That is, we consider the eigenvalue equation (46) for perturbations of the form $\delta\hat{\phi}(\mathbf{x}_\perp)=\delta\hat{\phi}(r)$, where r is the radial distance from the beam axis. We further introduce the (dimensionless) scaled variables defined by

$$\begin{aligned}&R=\frac{r}{r_b},\ K_z=k_zr_b,\ \Gamma_D=\frac{\lambda_{D\perp}}{r_b},\\&\Omega_p^2(R)=\frac{\omega_{pb}^2(r)}{\hat{\omega}_{pb}^2},\ \hat{\Omega}^2=\frac{(\omega-k_zV_b)^2}{\hat{\omega}_{pb}^2},\end{aligned} \tag{48}$$

where $\omega_{pb}^2(r)=4\pi n^0(r)q^2/\gamma_bm$ is the relativistic plasma frequency-squared. Note from Eq. (48) that lengths are scaled to the beam radius r_b, where $r_b/\lambda_{D\perp}$ is determined self-consistently in terms of $s_b=\hat{\omega}_{pb}^2/2\gamma_b^2\omega_{\beta\perp}^2$ from Eq. (22), and that frequencies are scaled to the on-axis $(r=0)$ plasma frequency $\hat{\omega}_{pb}=(4\pi\hat{n}q^2/\gamma_bm)^{1/2}$. From Eqs. (21) and (48), the normalized profile for $\Omega_{pb}^2(R)$ is given by

$$\Omega_p^2(R)=\begin{cases}\dfrac{I_0(\Gamma_D^{-1})-I_0(R/\Gamma_D)}{I_0(\Gamma_D^{-1})-1}, & 0\leqslant R<1,\\ 0, & 1<R<r_w/r_b.\end{cases} \tag{49}$$

Here, $\Gamma_D\equiv\lambda_{D\perp}/r_b$, and the outer edge of the beam $(r=r_b)$ corresponds to $R=r/r_b=1$. Note from Eq. (49) that $\Omega_p^2(R)$ decreases monotonically from unity at the beam axis $(R=0)$, to zero at the beam edge $(R=1)$. Moreover, for a low-intensity, moderate-emittance beam equilibrium with $\Gamma_D>1$ and $s_b\ll1$, Eq. (49) gives, to good approximation, the parabolic profile $\Omega_p^2(R)=1-R^2$, for $0\leqslant R<1$. On the other hand, for a high-intensity, low-emittance beam with $\Gamma_D\ll1$, and $s_b\to1$, Eq. (49) gives (approximately) the unit step-function profile, $\Omega_p^2(R)=1$, for $0\leqslant R<1$.

We now make use of Eq. (48) and the assumption $(\partial/\partial\theta)\delta\hat{\phi}(\mathbf{x}_\perp)=0$ to simplify the $\hat{T}_\parallel=0$ eigenvalue equation (46). Substituting $\boldsymbol{\nabla}_\perp\nabla_\perp^2\delta\hat{\phi}(r)=\hat{\mathbf{e}}_r[r^{-1}(\partial/\partial r)(r\partial/\partial r)-1/r^2](\partial/\partial r)\delta\hat{\phi}(r)$, where $\hat{\mathbf{e}}_r=\hat{\mathbf{e}}_x\cos\theta+\hat{\mathbf{e}}_y\sin\theta$ is a unit vector in the radial direction, some straightforward algebra shows that Eq. (46) can be expressed as

$$\begin{aligned}\frac{1}{R}\frac{\partial}{\partial R}R\Bigg\{&\left[\hat{\Omega}^2-\frac{\Omega_{pb}^2(R)}{\gamma_b^2}(1+K_z^2\Gamma_D^2)\right]\frac{\partial}{\partial R}\delta\hat{\phi}(R)\\&+\Gamma_D^2\frac{\Omega_{pb}^2(R)}{\gamma_b^2}\left(\frac{1}{R}\frac{\partial}{\partial R}R\frac{\partial}{\partial R}-\frac{1}{R^2}\right)\frac{\partial}{\partial R}\delta\hat{\phi}(R)\\&+\frac{1}{2}K_z^2\Gamma_D^2\frac{\partial}{\partial R}\left(\frac{\Omega_{pb}^4(R)/\gamma_b^2}{\hat{\Omega}^2}\delta\hat{\phi}(R)\right)\Bigg\}\\&-K_z^2[\hat{\Omega}^2-\Omega_{pb}^2(R)]\delta\hat{\phi}(R)=0.\end{aligned} \tag{50}$$

For $K_z=0$ and $\Gamma_D\neq0$, it is found that Eq. (50) gives purely stable oscillations with $Im\hat{\Omega}=0$ (Sec. IV B). On the other hand, as $K_z=k_zr_b$ is increased to sufficiently large values, the temperature anisotropy $(\hat{T}_\perp\propto\Gamma_D^2\neq0$, and $\hat{T}_\parallel=0)$ provides the free energy to drive an instability at moderate values of beam intensity (Sec. IV C).

B. Stable oscillations for $K_z=0$ and $\Gamma_D\neq 0$

Setting $K_z=0$, which corresponds to zero axial wavenumber ($k_z=0$), the eigenvalue equation (50) reduces to

$$\frac{1}{R}\frac{\partial}{\partial R}R\left\{\left[\hat{\Omega}^2-\frac{\Omega_p^2(R)}{\gamma_b^2}\right]\frac{\partial}{\partial R}\delta\hat{\phi}(R) + \Gamma_D^2\frac{\Omega_{pb}^2(R)}{\gamma_b^2}\left(\frac{1}{R}\frac{\partial}{\partial R}R\frac{\partial}{\partial R}-\frac{1}{R^2}\right)\frac{\partial}{\partial R}\delta\hat{\phi}(R)\right\}=0 \quad (51)$$

over the interval $0\leq R\leq R_w\equiv r_w/r_b$. We define $\delta\hat{E}_r(R)=-(\partial/\partial R)\delta\hat{\phi}(R)$, and denote the interior region of the beam ($0\leq R<1$) where $\Omega_{pb}^2(R)\neq 0$ by Region I, and the vacuum region exterior to the beam ($1<R\leq r_w/r_b$) where $\Omega_{pb}^2(R)=0$ by Region II. The eigenvalue equation (51) is readily integrated once with respect to R to give

$$\left\{\left[\hat{\Omega}^2-\frac{\Omega_{pb}^2(R)}{\gamma_b^2}\right]+\Gamma_D^2\frac{\Omega_{pb}^2(R)}{\gamma_b^2}\left(\frac{1}{R}\frac{\partial}{\partial R}R\frac{\partial}{\partial R}-\frac{1}{R^2}\right)\right\} \times\delta\hat{E}_r^{\rm I}(R)=0, \quad 0\leq R<1, \quad (52)$$

and

$$\delta\hat{E}_r^{\rm II}(R)=0,\ 1<R\leq r_w/r_b. \quad (53)$$

That is, the perturbed radial electric field is equal to zero outside the beam, with $\delta\hat{E}_r^{\rm II}(R)=0$, whereas the perturbed radial electric field inside the beam, $\delta\hat{E}_r^{\rm I}(R)$, satisfies Eq. (52). The solution to Eq. (52) in Region I is required to be regular at the origin ($R=0$) and continuous with the solution in Region II at the beam edge ($R=1$). Therefore, the eigenvalue equation (52) is to be solved subject to the boundary conditions

$$\delta\hat{E}_r^{\rm I}(R=0)=0=\delta\hat{E}_r^{\rm I}(R=1). \quad (54)$$

Equation (52) has been solved for the eigenfunction $\delta\hat{E}_r^{\rm I}(R)$ and eigenfrequency-squared $\hat{\Omega}^2$ subject to the boundary conditions in Eq. (52) using two approaches: (a) direct numerical integration of Eq. (52) using a shooting method to determine both the eigenfunctions and eigenvalues that are consistent with Eqs. (52) and (54), and (b) a matrix-dispersion-equation technique that expands Eq. (52) in a complete set of basis functions that satisfy *a priori* the boundary conditions in Eq. (54). The results using both approaches are in excellent agreement.

We illustrate here the matrix dispersion technique for solving Eq. (52). The boundary conditions in Eq. (54) and the occurrence of the Bessel-function operator $\Gamma_D^2[R^{-1}(\partial/\partial R)(R\partial/\partial R)-1/R^2]$ in Eq. (52), are strongly suggestive of expanding Eq. (52) in the complete set of basis functions $\{\alpha_n(R)\}$ where

$$\alpha_n(R)=A_nJ_1(\lambda_nR/\Gamma_D). \quad (55)$$

Here, $J_1(x)$ is the Bessel function of the first kind of order unity, $R/\Gamma_D=r/\lambda_{D\perp}$ in dimensional variables, $A_n=\sqrt{2}/J_2(\lambda_nr_b/\lambda_{D\perp})$ is a normalization constant, and λ_n is the nth zero of $[J_1(\lambda_nR/\Gamma_D)]_{R=1}=0$, i.e.,

$$J_1(\lambda_nr_b/\lambda_{D\perp})=0. \quad (56)$$

Note that $\{\alpha_n(R)\}$ form a complete set of basis functions on the interval $0\leq R\leq 1$ (or equivalently, $0\leq r\leq r_b$), with

$$\alpha_n(R=0)=0=\alpha_n(R=1), \qquad \int_0^1 dRR\alpha_n(R)\alpha_{n'}(R)=\delta_{n,n'}, \quad (57)$$

where $\delta_{n,n'}=1$ for $n=n'$, and $\delta_{n,n'}=0$ for $n\neq n'$. We represent the perturbed radial electric field $\delta\hat{E}_r^{\rm I}(R)$ in the beam interior ($0\leq R<1$) by

$$\delta\hat{E}_r^{\rm I}(R)=\sum_{n=1}^{\infty}\psi_n\alpha_n(R), \quad (58)$$

where $\{\psi_n\}$ are constant expansion coefficients, the eigenfunction $\alpha_n(R)$ solves

$$\Gamma_D^2\left(\frac{1}{R}\frac{\partial}{\partial R}R\frac{\partial}{\partial R}-\frac{1}{R^2}\right)\alpha_n(R)=-\lambda_n^2\alpha_n(R), \quad (59)$$

and λ_n is the nth zero of Eq. (56). Substituting Eqs. (58) and (59) into the eigenvalue equation (52) gives

$$\sum_{n=1}^{\infty}[\hat{\Omega}^2-(1+\lambda_n^2)\Omega_{pb}^2(R)/\gamma_b^2]\psi_n\alpha_n(R)=0 \quad (60)$$

for $0\leq R<1$.

Equation (60) is fully equivalent to the eigenvalue equation (52) in the beam interior, and automatically incorporates the boundary conditions in Eq. (54) by virtue of Eq. (57). Operating on Eq. (60) with $\int_0^1 dRR\alpha_m(R)\ldots$, we obtain

$$\sum_{n=1}^{\infty}D_{n,m}(\hat{\Omega}^2)\psi_n=0, \quad (61)$$

where the matrix elements $D_{n,m}(\hat{\Omega}^2)$ are defined by

$$D_{n,m}(\hat{\Omega}^2)=\gamma_b^2\hat{\Omega}^2\delta_{n,m}-(1+\lambda_n^2)C_{n,m}, \quad (62)$$

and the constants $C_{n,m}$ are defined by

$$C_{n,m}=\int_0^1 dRR\Omega_{pb}^2(R)\alpha_n(R)\alpha_m(R). \quad (63)$$

The requirement that Eq. (61) has a nontrivial solution ($\psi_n\neq 0$ for some n) gives the matrix dispersion relation

$$\det\{D_{n,m}(\hat{\Omega}^2)\}=0. \quad (64)$$

Equation (64) determines the normalized oscillation frequency $\hat{\Omega}=\Omega/\hat{\omega}_{pb}$ as a function of the system parameters $s_b=\hat{\omega}_{pb}^2/2\gamma_b^2\omega_{b\perp}^2$ and $\lambda_{D\perp}/r_b$, which are related by Eq. (22) (see Fig. 2). Furthermore, the normalized profile for $\Omega_{pb}^2(R)$ occurring in the definition of $C_{n,m}$ in Eq. (63) is defined in terms of $\Gamma_D=\lambda_{D\perp}/r_b$ and $R=r/r_b$ in Eq. (49).

The matrix dispersion relation (64), valid for zero axial wavenumber ($k_z=0$), can be used to calculate the normal mode oscillation frequencies for perturbations about a warm-fluid waterbag equilibrium with $\hat{T}_\parallel=0$. The solutions to Eq. (64) are a discrete set of stable modes $\{\Omega_n/\hat{\omega}_{pb}\}$, $n=1,2,3,...$, with $Im\,\Omega_n=0$, and the dimension N of the matrix

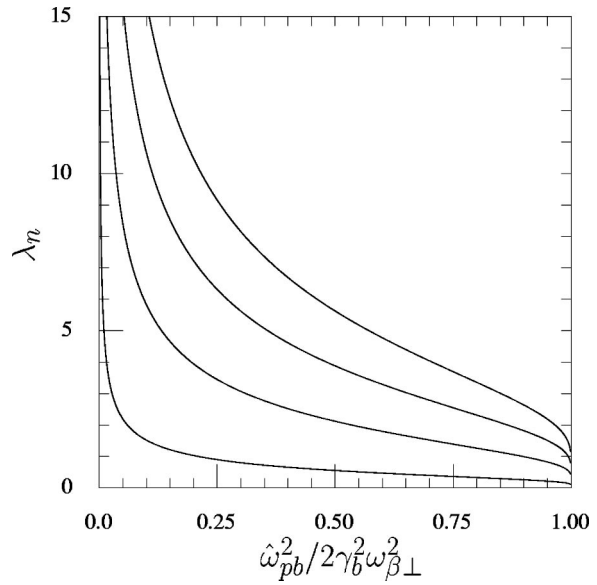

FIG. 3. Plots of λ_n versus $\hat{\omega}_{pb}^2/2\gamma_b^2\omega_{\beta\perp}^2$ obtained from Eqs. (22) and (65) for mode numbers $n=1,2,...,4$. Here, $\lambda_n=\Gamma_n\lambda_{D\perp}/r_b$, where $J_1(\Gamma_n)=0$.

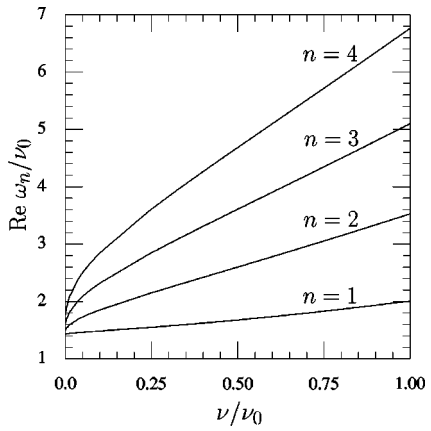

FIG. 4. Plots of $Re\,\omega_n/\nu_0$ versus ν/ν_0 for mode numbers $n=1,2,...,4$ obtained numerically from the matrix dispersion equation (64). Here, $\nu_0 \equiv \omega_{\beta\perp}$, and $\nu/\nu_0=(1-\hat{\omega}_{pb}^2/2\gamma_b^2\omega_{\beta\perp}^2)^{1/2}$ is a measure of the depressed tune.

required to solve Eq. (64) numerically for $\{\Omega_n/\hat{\omega}_{pb}\}$ to good accuracy depends on the order of the mode of interest. For example, to determine $\Omega_n/\hat{\omega}_{pb}$ for radial mode number n to an accuracy of one part in 10^3 in a tenuous beam, it is adequate to consider a $3n\times 3n$ approximation to the matrix dispersion relation [Eq. (64)] with $N=3n$. Greater accuracies can be achieved with much smaller matrices for more intense beams, since the matrix is closer to diagonal. In this regard, at very high beam intensities when $s_b=\hat{\omega}_{pb}^2/2\gamma_b^2\omega_{\beta\perp}^2\to 1$, it is important to note from Eqs. (21), (22), and (49) (see also Figs. 1 and 2) that $\Omega_{pb}^2(R)$ approaches the constant unit step function on the interval $0\leqslant R<1$. In this case, for $\hat{\omega}_{pb}^2/2\gamma_b^2\omega_{\beta\perp}^2\to 1$, it follows from Eqs. (57) and (63) that $C_{n,m}\to\delta_{n,m}$, and the matrix $\{D_{n,m}(\hat{\Omega}^2)\}$ becomes diagonal to good approximation. It is also clear from Eqs. (62) and (64) that the values of $\{\lambda_n\}$ play an important role in determining the normal-mode oscillation frequencies $\{\Omega_n/\hat{\omega}_{pb}\}$. Here, λ_n is the nth zero of $J_1(\lambda_n r_b/\lambda_{D\perp})=0$ [Eq. (56)]. We define

$$\lambda_n=\frac{\lambda_{D\perp}}{r_b}\Gamma_n, \tag{65}$$

where $\{\Gamma_n\}$ are the (tabulated) solutions to $J_1(\Gamma_n)=0$, and $\lambda_{D\perp}/r_b$ is determined self-consistently in terms of the normalized beam intensity $s_b=\hat{\omega}_{pb}^2/2\gamma_b^2\omega_{\beta\perp}^2$ by Eq. (22) (Fig. 2). Since $\{\Gamma_n\}$ have constant numerical values, it follows from Eqs. (22) and (65) that the values of $\{\lambda_n\}$ depend on the normalized beam intensity $s_b=\hat{\omega}_{pb}^2/2\gamma_b^2\omega_{\beta\perp}^2$. Shown in Fig. 3 are plots of λ_n versus $\hat{\omega}_{pb}^2/2\gamma_b^2\omega_{\beta\perp}^2$ for mode numbers $n=1,2,...,4$, obtained numerically from Eqs. (22) and (55). As expected, the curves in Fig. 3 are similar in shape to the curve in Fig. 2, scaled by the constant factor Γ_n, for $n=1,2,...,4$.

We now present numerical solutions to the matrix dispersion equation (64) (Fig. 4) for mode numbers $n=1,2,...,4$. In this regard, it is convenient to introduce the characteristic measures of the depressed and undepressed single-particle transverse oscillation frequencies, ν and ν_0, defined by

$$\nu^2\equiv\omega_{\beta\perp}^2-\hat{\omega}_{pb}^2/2\gamma_b^2, \quad \nu_0^2\equiv\omega_{\beta\perp}^2, \tag{66}$$

and the effective tune depression, ν/ν_0, where

$$\frac{\nu^2}{\nu_0^2}=1-\frac{\hat{\omega}_{pb}^2}{2\gamma_b^2\omega_{\beta\perp}^2}=1-s_b. \tag{67}$$

Using a 10×10 matrix representation, the numerical solutions to Eq. (64) are presented in Fig. 4 for mode numbers $n=1,2,...,4$. Here, the solutions for $\Omega_n=\omega_n$ are purely real ($Im\,\omega_n=0$), and $Re\,\omega_n/\nu_0$ is plotted versus ν/ν_0 in Fig. 4 for effective tune depressions ranging from $\nu/\nu_0=0$ ($s_b=1$) to $\nu/\nu_0=1$ ($s_b=0$). For each value of n, note that the $\nu/\nu_0=0$ ($\hat{\omega}_{pb}^2/2\gamma_b^2\omega_{\beta\perp}^2=1$) intercept in Fig. 4 corresponds to the single frequency $Re\,\omega_n=\sqrt{2}\nu_0=\sqrt{2}\omega_{\beta\perp}=\hat{\omega}_{pb}/\gamma_b$ in the limit of high beam intensity. On the other hand, as $\nu/\nu_0=(1-s_b)^{1/2}$ is increased (decreasing beam intensity $s_b=\hat{\omega}_{pb}^2/2\gamma_b^2\omega_{\beta\perp}^2$), it is evident from Fig. 4 that there is a discrete spectrum of stable oscillations with frequencies $\{\omega_n\}$ that increase as ν/ν_0 and n are increased. The general features of the solutions for $\{\omega_n\}$ presented in Fig. 4 for $k_z=0$ perturbations about a warm-fluid waterbag equilibrium are qualitatively similar to those for a warm-fluid Kapchinskij–Vladimirskij (KV) equilibrium,[50] although the precise values of $\{\omega_n\}$ differ as ν/ν_0 is increased. For completeness, shown in Fig. 5 are plots of the eigenfunction $\delta\hat{E}_r^I(r)$ versus r/r_b for radial mode numbers $n=1,2,3$ obtained numerically from Eqs. (58), (60), and (64) for $s_b=0.36$ and $\nu/\nu_0=0.8$. Note from Fig. 5 that the number of radial oscillations of $\delta\hat{E}_r^I(r)$ increase as the mode number n is increased. Moreover, for specified mode number n, the number of ''zeros'' of $\delta\hat{E}_r^I(r)$ in the interval $0\leqslant r\leqslant r_b$ is equal to $n+1$. Finally, for the numerical results presented in Figs. 4 and 5, we have used a 10×10 representation of the matrix equations in Eqs. (58), (60), and (64).

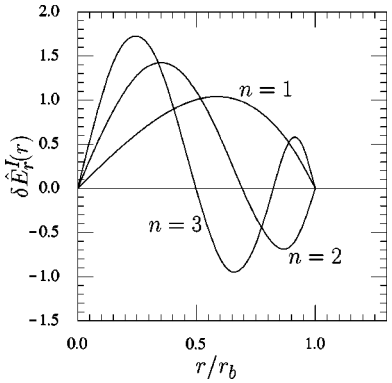

FIG. 5. Plots of the eigenfunction $\delta\hat{E}_r^{\rm I}(r)$ versus r/r_b for radial mode numbers $n=1,2,3$ obtained numerically from Eqs. (58), (60), and (64) for $s_b=0.36$ and $\nu/\nu_0=0.8$, using a 10×10 representation of the matrix equations.

C. Stability properties for $K_z\neq0$ and $\Gamma_D\neq0$

We now examine the $\hat{T}_\parallel=0$ eigenvalue equation (50) for the general case where the normalized axial wavenumber $K_z=k_zr_b$ is nonzero ($k_z\neq0$). In this case, the eigenvalue equation is more complicated than Eq. (51) and must generally be solved using numerical shooting techniques. In Region I (the beam interior), where $\Omega_{pb}^2(R)\neq0$, Eq. (50) can be expressed as

$$\frac{1}{R}\frac{\partial}{\partial R}R\Bigg\{\left[\hat{\Omega}^2-\frac{\Omega_{pb}^2(R)}{\gamma_b^2}(1+K_z^2\Gamma_D^2)\right]\frac{\partial}{\partial R}\delta\hat{\phi}^{\rm I}(R)$$
$$+\Gamma_D^2\frac{\Omega_{pb}^2(R)}{\gamma_b^2}\left(\frac{1}{R}\frac{\partial}{\partial R}R\frac{\partial}{\partial R}-\frac{1}{R^2}\right)\frac{\partial}{\partial R}\delta\hat{\phi}^{\rm I}(R)$$
$$+\frac{1}{2}K_z^2\Gamma_D^2\frac{\partial}{\partial R}\left(\frac{\Omega_{pb}^4(R)/\gamma_b^2}{\hat{\Omega}^2}\delta\hat{\phi}^{\rm I}(R)\right)\Bigg\}$$
$$-K_z^2[\hat{\Omega}^2-\Omega_{pb}^2(R)]\delta\hat{\phi}^{\rm I}(R)=0,\quad 0\leqslant R<1, \tag{68}$$

where $\hat{\Omega}^2\equiv\Omega^2/\hat{\omega}_{pb}^2$, $\Gamma_D\equiv\lambda_{D\perp}/r_b$, $R\equiv r/r_b$, $K_z\equiv k_zr_b$, and $\Omega_{pb}^2(R)$ is defined in Eq. (49). On the other hand, in Region II (the vacuum region outside the beam), where $\Omega_{pb}^2(R)=0$, Eq. (50) becomes

$$\frac{1}{R}\frac{\partial}{\partial R}R\frac{\partial}{\partial R}\delta\hat{\phi}^{\rm II}(R)-K_z^2\delta\hat{\phi}^{\rm II}(R)=0,\ 1<R\leqslant R_w, \tag{69}$$

where $R_w\equiv r_w/r_b$. Equation (69) is a modified Bessel's equation of order zero, and the solution that satisfies $\delta\hat{\phi}^{\rm II}(R=R_w)=0$ and is continuous with the solution $\delta\hat{\phi}^{\rm I}(R)$ at the beam edge ($R=1$) is given by

$$\delta\hat{\phi}^{\rm II}(R)=\delta\hat{\phi}^{\rm I}(R=1)$$
$$\times\frac{I_0(K_zR)K_0(K_zR_w)-K_0(K_zR)I_0(K_zR_w)}{I_0(K_z)K_0(K_zR_w)-K_0(K_z)I_0(K_zR_w)},$$
$$1<R\leqslant R_w, \tag{70}$$

where $I_0(x)$ and $K_0(x)$ are modified Bessel functions of the first and second kinds, respectively, of order zero. In Eq. (70), $\delta\hat{\phi}^{\rm I}(R=1)\equiv\lim_{\epsilon\to0_+}[\delta\hat{\phi}^{\rm I}(R)]_{R=1-\epsilon}$, where $\delta\hat{\phi}^{\rm I}(R)$ is the solution to Eq. (68) in the beam interior ($0\leqslant R<1$). The remaining boundary condition at the beam edge is obtained by integrating the eigenvalue equation (68) across the beam surface at $R=1$. In this regard, we make use of the fact that the profile for $\Omega_{pb}^2(R)$ approaches zero continuously as $R=r/r_b$ approaches unity (from below), except in the singular limit where $s_b=\hat{\omega}_{pb}^2/2\gamma_b^2\omega_{\beta\perp}^2=1$ and $\lambda_{D\perp}=0$. Operating on Eq. (68) with $\int_{1-\epsilon}^{1+\epsilon}dRR\ldots$, taking the limit $\epsilon\to0_+$, and making use of $[\Omega_{pb}^2(R=1-\epsilon)]_{\epsilon\to0_+}=0$ and the continuity of $\delta\hat{\phi}(R)$ at $R=1$, we obtain

$$\lim_{\epsilon\to0_+}\left[\frac{\partial}{\partial R}\delta\hat{\phi}^{\rm I}(R)\right]_{R=1-\epsilon}=\lim_{\epsilon\to0_+}\left[\frac{\partial}{\partial R}\delta\hat{\phi}^{\rm II}(R)\right]_{R=1+\epsilon}. \tag{71}$$

Equation (71) corresponds to continuity of the perturbed radial electric field at the beam surface, i.e., there is no surface-charge perturbation at $R=1$ for the warm-fluid waterbag equilibrium profile for $\Omega_{pb}^2(R)$ in Eq. (49). Substituting the solution for $\delta\hat{\phi}^{\rm II}(R)$ in Eq. (70) into Eq. (71) gives

$$\left[\frac{\partial}{\partial R}\delta\hat{\phi}^{\rm I}(R)\right]_{R=1}$$
$$=K_z\delta\hat{\phi}^{\rm I}(R=1)\frac{K_0(K_zR_w)I_0'(K_z)-K_0'(K_z)I_0(K_zR_w)}{K_0(K_zR_w)I_0(K_z)-K_0(K_z)I_0(K_zR_w)}, \tag{72}$$

where $I_0'(x)=(d/dx)I_0(x)$, etc., $R_w=r_w/r_b$ and $K_z=k_zr_b$.

In Eq. (72), the solution to Eq. (68) for $\delta\hat{\phi}^{\rm I}(R)$ in the interval $0\leqslant R<1$ depends on both the radial coordinate $R=r/r_b$ and the normalized frequency $\hat{\Omega}=(\omega-k_zV_b)/\hat{\omega}_{pb}$, as well as the normalized axial wavenumber $K_z=k_zr_b$ and other system parameters such as $\lambda_{D\perp}/r_b$ and $\hat{\omega}_{pb}^2/2\gamma_b^2\omega_{\beta\perp}^2$. Therefore, once the solution for $\delta\hat{\phi}^{\rm I}(R)$ is determined numerically from Eq. (68), the boundary condition at $R=1$ in Eq. (72) effectively plays the role of a *dispersion relation* that determines the complex oscillation frequency $(\omega-k_zV_b)/\hat{\omega}_{pb}$ as a function of k_zr_b and other system parameters. We introduce the geometric factor g_0 defined by

$$\frac{1}{g_0}=k_zr_b\frac{K_0(k_zr_w)I_0'(k_zr_b)-K_0'(k_zr_b)I_0(k_zr_w)}{K_0(k_zr_w)I_0(k_zr_b)-K_0(k_zr_b)I_0(k_zr_w)}, \tag{73}$$

where $k_zr_b=K_z$ and $k_zr_w=K_zR_w$. Equation (72) can then be expressed as

$$D(\Omega/\hat{\omega}_{pb})\equiv\left[\frac{\partial}{\partial R}\delta\hat{\phi}^{\rm I}(R)\right]_{R=1}-\frac{1}{g_0}\delta\hat{\phi}^{\rm I}(R=1)=0. \tag{74}$$

Equation (68) is a *linear* equation for $\delta\hat{\phi}^{\rm I}(R)$, which can be scaled by a constant amplitude factor. Therefore, as noted earlier, $D(\Omega/\hat{\omega}_{pb})=0$, plays the role of a dispersion relation which determines the complex oscillation frequency $\Omega/\hat{\omega}_{pb}=(\omega-k_zV_b)/\hat{\omega}_{pb}$. For future reference, the geometric factor g_0 defined by Eq. (73) can be approximated by

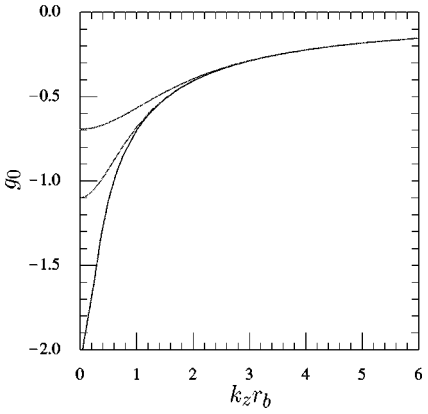

FIG. 6. Plots of the geometric factor g_0 defined in Eq. (73) versus $k_z r_b$ for $r_b/r_w=1/2$, $r_b/r_w=1/3$, and $r_b/r_w=1/8$.

$$g_0=\begin{cases} -\ln\left(\dfrac{r_w}{r_b}\right), & \text{for } k_z^2 r_w^2 \ll 1, \\ -\dfrac{1}{k_z r_b}, & \text{for } k_z^2 r_b^2 \gg 1, \end{cases} \tag{75}$$

in the limits of long and short axial wavelengths. Shown in Fig. 6 is a plot of g_0 versus $k_z r_b$ obtained from Eq. (73) for the three cases, $r_b/r_w=1/2$, $r_b/r_w=1/3$, and $r_b/r_w=1/8$.

D. Numerical solution for $K_z \neq 0$ and $\Gamma_D \neq 0$

The eigenvalue equation (68) is a linear fourth-order ordinary differential equation. At $R=0$, several of the coefficients are singular. At $R=1$, the beam edge, the coefficient multiplying the highest-derivative term vanishes, causing a boundary layer. Since standard numerical integration techniques are not applicable, we instead expand the solution near $R=0$ in a Froebenius series. Using this analytical expansion near the origin where it is sufficiently accurate, we begin by numerically integrating from very near $R=0$ out to the beam edge at $R=1$, and also from near $R=0$, back to the origin.

In stable regimes, the eigenfrequencies are real, and so the imaginary part of the eigenfunction, if chosen to be zero at the origin, is zero everywhere. For unstable modes, the complex eigenfrequency links the evolution of the real and imaginary parts of the eigenfunction in Eq. (50). Exterior to the beam ($1<R\leqslant R_w$), the eigenfunction $\delta\hat{\phi}^{\rm II}(R)$ takes the form in Eq. (70), which has constant complex phase out to the wall.

The linearity of Eq. (68) implies that the solution for $\delta\hat{\phi}^{\rm I}(R)$ is arbitrary up to a constant, multiplicative, complex factor. This freedom can be used in the unstable case to make the matching of real and imaginary parts at the beam edge simpler. For present purposes, we choose the initial amplitude and phase at $R=0$ such that $Re[\,\delta\hat{\phi}^{\rm I}(R=0)]=1$ and $Im[\,\delta\hat{\phi}^{\rm I}(R=0)]=0$. In the unstable case, integrating away from $R=0$, the eigenfunction generally develops an imaginary component with $Im[\,\delta\hat{\phi}^{\rm I}(R)]\neq 0$. Of course at the beam edge ($R=1$), there are four conditions to satisfy, corresponding to continuity of $\delta\hat{\phi}(R)$,

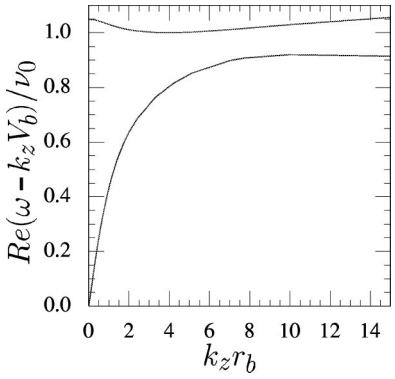

FIG. 7. Plots of $Re(\omega-k_z V_b)/\nu_0$ versus $k_z r_b$ obtained numerically from Eqs. (68), (70), (76) and (77) for $\Gamma_D=0.360$ ($s_b=0.755$).

$$\begin{aligned} Re[\,\delta\hat{\phi}^{\rm I}(R=1)]&=Re[\,\delta\hat{\phi}^{\rm II}(R=1)], \\ Im[\,\delta\hat{\phi}^{\rm I}(R=1)]&=Im[\,\delta\hat{\phi}^{\rm II}(R=1)], \end{aligned} \tag{76}$$

and continuity of $(\partial/\partial R)\,\delta\hat{\phi}(R)$ [see also Eq. (71)],

$$\begin{aligned} Re\left[\frac{\partial}{\partial R}\,\delta\hat{\phi}^{\rm I}(R)\right]_{R=1}&=Re\left[\frac{\partial}{\partial R}\,\delta\hat{\phi}^{\rm II}(R)\right]_{R=1}, \\ Im\left[\frac{\partial}{\partial R}\,\delta\hat{\phi}^{\rm I}(R)\right]_{R=1}&=Im\left[\frac{\partial}{\partial R}\,\delta\hat{\phi}^{\rm II}(R)\right]_{R=1}. \end{aligned} \tag{77}$$

We can automatically satisfy the matching conditions in Eq. (76) by appropriate choice of complex phase factor for the solution for $\delta\hat{\phi}^{\rm II}(R)$ in Eq. (70). In general, however, neither of the matching conditions on $\partial\,\delta\hat{\phi}/\partial R$ at $R=1$ in Eq. (77) will be satisfied unless the complex eigenfrequency $\Omega=\Omega_r+i\Omega_i$ occurring in Eq. (68) is correctly chosen, which corresponds to the dispersion relation in Eq. (74). Therefore, in the present shooting method, Eq. (68) is repeatedly integrated, and the value of $\Omega_r+i\Omega_i$ adjusted until the matching conditions in Eq. (77) are satisfied, thereby determine the desired eigenfrequency.

Using this method, Eqs. (68) and (70) have been solved numerically subject to the boundary conditions in Eqs. (76) and (77), and the complex eigenfrequency $\Omega=\Omega_r+i\Omega_i$ and eigenfunction $\delta\hat{\phi}(R)$ have been determined self-consistently over a wide range of system parameters corresponding to normalized beam intensity, $s_b=\hat{\omega}_{pb}^2/2\gamma_b^2\omega_{\beta\perp}^2$, tune depression, $\nu/\nu_0=(1-s_b)^{1/2}$, transverse Debye length, $\Gamma_D=\lambda_{D\perp}/r_b$, and axial wavenumber, $K_z=k_z r_b$. Here, keep in mind that s_b and Γ_D are related by Eq. (22), so that very high beam intensity ($s_b\to 1$) corresponds to $\Gamma_D\ll 1$, and low beam intensity ($s_b\ll 1$) corresponds to $\Gamma_D\gg 1$ (see Fig. 2). Because $\hat{T}_\parallel=0$ is assumed in the present analysis, the term proportional to $K_z^2\Gamma_D^2\neq 0$ in Eq. (68) provides the free energy to drive instability associated with temperature anisotropy ($\hat{T}_\perp>\hat{T}_\parallel$). Typical numerical results obtained from Eqs. (68), (70), (76), and (77) are illustrated in Figs. 7–13 for a mildly relativistic beam with $\gamma_b=1.02$ and $r_w/r_b=2$. As a general remark, beams which are cold in the transverse direction oscillate stably at all values of axial wavelength. Beams with intermediate transverse temperatures are un-

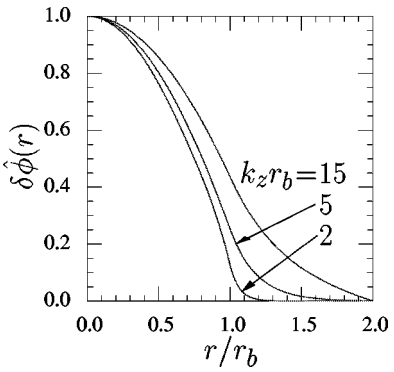

FIG. 8. Plots of eigenfunction $\delta\hat{\phi}(r)$ versus r/r_b for several values of $k_z r_b$ for the choice of system parameters in Fig. 7.

stable for *all* wavenumbers $k_z r_b$ larger than a critical value. Finally, beams which are sufficiently hot in the transverse direction have a *finite* instability bandwidth in $k_z r_b$: shorter wavelengths and long wavelengths are stable, while wavelengths in a range about $k_z r_b \Gamma_D \sim 1$ are unstable. That is, the growth rate of sufficiently temperature-dominated beams turns over and approaches zero at large values of $k_z r_b$. (From the analysis in Sec. IV B, keep in mind that the system is stable for $k_z = 0$.) For the choice of waterbag equilibrium considered here with $\hat{T}_\parallel = 0$, the onset of instability occurs for

$$\Gamma_D > \Gamma_D^* = 0.364, \quad s_b < s_b^* = 0.750, \quad \frac{\nu}{\nu_0} > \frac{\nu^*}{\nu_0} = 0.500. \quad (78)$$

The inequalities in Eq. (78) are equivalent conditions [see Eqs. (22), (67), and Fig. 2]. For increasing values of Γ_D relative to Γ_D^*, the instability bandwidth first increases, encompassing both higher and lower axial wavenumbers. For even warmer beams, however, high values of $k_z r_b$ become stabilized, while the region of instability continues to shift to smaller axial wavenumbers.

Figures 7 and 8 show typical numerical results for the choice of system parameters $\Gamma_D = 0.360$ ($s_b = 0.755$), corresponding to *stable* oscillations with $Im\Omega = Im\omega = 0$. Plotted in Fig. 7 is $Re(\omega - k_z V_b)/\nu_0$ versus $k_z r_b$ for the $n = 1$ eigenmode, whereas Fig. 8 shows the corresponding eigenfunction $\delta\hat{\phi}(r)$ (assumed real) plotted versus r/r_b for several values of $k_z r_b$. The high-frequency (upper) branch in Fig. 7 corresponds to the familiar plasma oscillation branch considered in Sec. IV B for $k_z = 0$, extended to nonzero values of $k_z r_b$. The lower (slow-wave) branch in Fig. 7 starts at zero frequency for $k_z = 0$, and $Re(\omega - k_z V_b)$ increases linearly with $k_z r_b$ for $k_z r_b < 1$, and then asymptotes at $Re(\omega - k_z V_b) \simeq 1.03\nu_0$ for $k_z r_b \gg 1$, for the choice of system parameters in Fig. 7. On the other hand, the upper (high-frequency) branch in Fig. 7 asymptotes at $Re(\omega - k_z V_b) \simeq 1.3\nu_0$ for $k_z r_b \gg 1$. From Fig. 8, as expected, for $k_z = 0$ the $n = 1$ eigenfunction $\delta\hat{\phi}(r)$ has a node precisely at the beam edge ($r = r_b$). On the other hand, as $k_z r_b$ is increased, the eigenfunction $\delta\hat{\phi}(r)$ extends radially well into the vacuum region, with $\delta\hat{\phi}(r = r_w) = 0$.

For $\Gamma_D > \Gamma_D^*$, the two branches in Fig. 7 coalesce as $k_z r_b$ is increased beyond some critical value $k_z^*(\Gamma_D) r_b$. Typical numerical results in this case are illustrated in Figs. 9–11 for the choice of system parameters $\Gamma_D = 0.509$ ($s_b = 0.55$). From Fig. 9, for $0 \leq k_z r_b < k_z^* r_b = 0.968$, the eigenvalue equation supports two real oscillatory solutions with $Im\omega = 0$. For $k_b r_b > k_z^* r_b = 0.968$, however, the two modes coalesce and have the same value of $Re(\omega - k_z V_b)$, and complex conjugate values of $Im\omega$ (one mode is damped, and the other is growing). The normalized growth rate $Im\omega/\nu_0$ of the unstable branch is plotted versus $k_z r_b$ in Fig. 9, and increases from $Im\omega = 0$ at $k_z r_b = k_z^* r_b = 0.968$, to $Im\omega \simeq 0.4\nu_0$ for $k_z r_b \gg 1$. Consistent with Fig. 9, the corresponding eigenfunction plots of $Re[\delta\hat{\phi}(r)]$ and $Im[\delta\hat{\phi}(r)]$ versus r/r_b are presented in Figs. 10 and 11 for several values of $k_z r_b$ corresponding to instability. For moderately low values of $k_z r_b$, the eigenfunction for the unstable mode has the distinctive $n = 1$ mode structure illustrated in Fig. 10 for $k_z r_b = 4$. As $k_z r_b$ is increased, however, the real part of the eigenfunction, $Re[\delta\hat{\phi}(r)]$, changes continuously from an $n = 1$ to an $n = 2$ mode structure as shown by the progression in Fig. 11. For very large $k_z r_b > 10$, the boundary layer at $r = r_b$ becomes very sharp, with large changes in $Re[\delta\hat{\phi}(r)]$ over a very short radial scale. The radial mode number, however, does not appear to change from $n = 2$. Of course, perturbations with such large values of $k_z r_b$ are of limited practical interest because the modes would be stabilized ($Im\omega = 0$) at short axial wavelengths by finite $\hat{T}_\parallel \neq 0$ effects in an

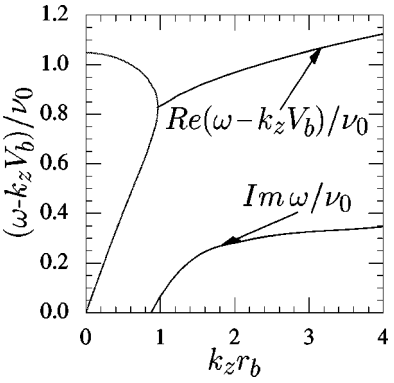

FIG. 9. Plots of $Re(\omega - k_z V_b)/\nu_0$ and $Im\omega/\nu_0$ versus $k_z r_b$ obtained numerically from Eqs. (68), (70), (76) and (77) for the choice of system parameters $\Gamma_D = 0.509$ ($s_b = 0.55$).

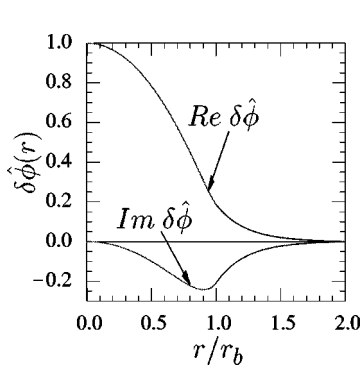

FIG. 10. Plots of $Re[\delta\hat{\phi}(r)]$ and $Im[\delta\hat{\phi}(r)]$ versus r/r_b for $k_z r_b = 4$ and the choice of system parameters in Fig. 9.

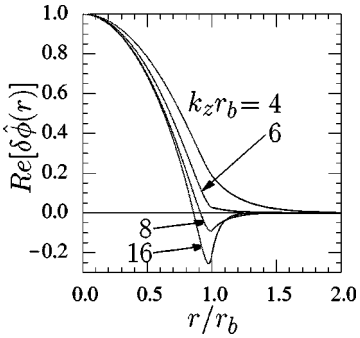

FIG. 11. Plots of $Re[\delta\hat{\phi}(r)]$ versus r/r_b for several values of $k_z r_b$ and the choice of system parameters in Fig. 9.

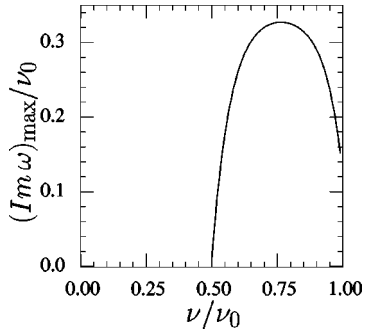

FIG. 13. Plot of $(Im\omega)_{max}/\nu_0$ versus $\nu/\nu_0=(1-s_b)^{1/2}$. (See also Fig. 12.)

analysis of the more complete eigenvalue equation (45).

For completeness, shown in Fig. 12 are plots of the normalized growth rate $Im\omega/\nu_0$ versus $k_z r_b$ obtained numerically from Eqs. (68), (70), (76), and (77) for several values of $\Gamma_D > \Gamma_D^*$ and $s_b < s_b^*$. Note from Fig. 12 that critical value of $k_z r_b$ for onset of instability increases as Γ_D is increased (s_b is decreased), and that the maximum normalized growth rate $(Im\omega)_{max}/\nu_0$ increases as Γ_D is increased (s_b is decreased). For sufficiently large values of Γ_D (large enough transverse emittance), we also note from Fig. 12 that the instability has a finite bandwidth in $k_z r_b$, whereas for smaller values of Γ_D, the maximum growth rate occurs for $k_z r_b \gg 1$. For $\hat{T}_\parallel \neq 0$ (but $\hat{T}_\parallel < \hat{T}_\perp$), it is expected that the more complete eigenvalue equation (45) will always give a finite instability bandwidth in $k_z r_b$. Finally, a corresponding plot of the maximum normalized growth rate $(Im\omega)_{max}/\nu_0$ versus depressed tune $\nu/\nu_0=(1-s_b)^{1/2}$ is shown in Fig. 13. Note from Fig. 13 that the onset of instability occurs for $\nu/\nu_0 > \nu^*/\nu_0 = 0.5$ for the choice of system parameters here [see Eq. (78)].

V. CONCLUSIONS

To briefly summarize, following a discussion of the macroscopic warm-fluid model and the waterbag equilibrium in Sec. II, we linearized the macroscopic fluid equations for small-amplitude perturbations in Sec. III, and derived a single eigenvalue equation for the perturbed electrostatic potential $\delta\phi(\mathbf{x},t)$, allowing for arbitrary anisotropy in the perpendicular and parallel pressures, $P_\perp^0(r)$ and $P_\parallel^0(r)$. Detailed stability properties were calculated numerically in Sec. IV for the case of extreme anisotropy with $P_\parallel^0(r)=0$ and $P_\perp^0(r)\neq 0$, assuming axisymmetric wave perturbations $(\partial/\partial\theta = 0)$ of the form $\delta\phi(\mathbf{x},t)=\delta\hat{\phi}(r)\exp(ik_z z - i\omega t)$, where k_z is the axial wavenumber, and $Im\omega > 0$ corresponds to instability (temporal growth). For $k_z = 0$, the analysis of the eigenvalue equation led to a discrete spectrum $\{\omega_n\}$ of stable oscillations with $Im\omega_n = 0$, where n is the radial mode number (Sec. IV B). On the other hand, for sufficiently large values of $k_z r_b$, where r_b is the beam radius, the analysis of the eigenvalue equation led to an anisotropy-driven instability $(Im\omega > 0)$ provided the normalized Debye length $(\Gamma_D = \lambda_{D\perp}/r_b)$ is sufficiently large and the normalized beam intensity $(s_b = \hat{\omega}_{pb}^2/2\gamma_b^2/2\gamma_b^2\omega_{\beta b}^2)$ is sufficiently below the space-charge limit (Sec. IV C). Depending on system parameters, it is found that the growth rate can be a substantial fraction of the applied focusing frequency $\omega_{\beta\perp}$.

In conclusion, application of a warm-fluid model to describe the equilibrium and stability properties of intense charged particle beams appears to be a remarkably robust and simple approach, both for the case of stable high-frequency oscillations considered by Lund and Davidson,[50] as well as the unstable case considered here, where the instability is driven by gross macroscopic properties of the beam equilibrium (pressure anisotropy).

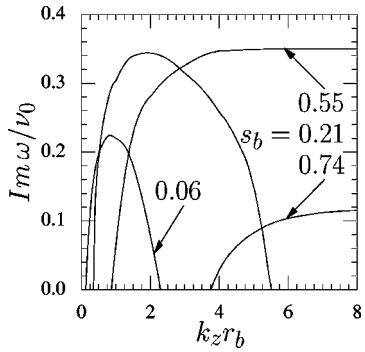

FIG. 12. Plots of $Im\omega/\nu_0$ versus $k_z r_b$ obtained numerically from Eqs. (68), (70), (76) and (77) for several values of $\Gamma_D > \Gamma_D^*$ and $s_b < s_b^*$.

ACKNOWLEDGMENT

This research was supported by the Department of Energy.

[1] R. C. Davidson, *Physics of Nonneutral Plasmas* (Addison-Wesley, Reading, MA, 1990), and references therein.
[2] T. P. Wangler, *Principles of RF Linear Accelerators* (Wiley, New York, 1998).
[3] H. Wiedemann, *Particle Accelerator Physics* (Springer, New York, 1993), vols. I and II.
[4] M. Reiser, *Theory and Design of Charged Particle Beams* (Wiley, New York, 1994).
[5] J. D. Lawson, *The Physics of Charged-Particle Beams* (Oxford Science, New York, 1988).
[6] See, for example, Proceedings of the 1995 International Symposium on Heavy Ion Inertial Fusion, edited by J. J. Barnard, T. J. Fessenden and E. P. Lee [Fusion Eng. Design **32**, 1–620 (1996)], and references therein.
[7] E. P. Lee and J. Hovingh, Fusion Technol. **15**, 369 (1989).
[8] A. Friedman, R. O. Bangerter, and W. B. Hermannsfeldt, in *Proceedings of the IAEA Technical Committee Meeting on Drivers for Inertial Confine-*

ment Fusion, Paris, France, 1994 (Commisariat a l'Energie Atomique, Saclay, France, 1995), p. 243.
[9]R. W. Muller, in *Nuclear Fusion by Inertial Confinement: A Comprehensive Treatise*, edited by G. Velarde, Y. Ronen, and J. M. Martinez-Val (CRC, Boca Raton, FL, 1993), chap. 17, pp. 437–453.
[10]R. A. Jameson, in *Advanced Accelerator Concepts, Port Jefferson, NY, 1992*, J. S. Wurtele [AIP Conf. Proc. **279**, 969 (American Institute of Physics, Melville, NY, 1993)].
[11]I. Kapchinskij and V. Vladimirskij, in *Proceedings of the International Conference on High Energy Accelerators and Instrumentation* (CERN Scientific Information Service, Geneva, 1959), p. 274.
[12]R. L. Gluckstern, in *Proceedings of the 1970 Proton Linear Accelerator Conference, Batavia, IL, 1971*, edited by M. R. Tracy (National Accelerator Laboratory, Batavia, IL, 1971), p. 811.
[13]H. S. Uhm and R. C. Davidson, Phys. Fluids **23**, 1586 (1980).
[14]H. S. Uhm and R. C. Davidson, Part. Accel. **11**, 65 (1980).
[15]T.-S. Wang and L. Smith, IEEE Trans. Nucl. Sci. **NS-28**, 2399 (1981).
[16]T.-S. Wang and L. Smith, Part. Accel. **12**, 247 (1982).
[17]I. Hofmann, L. J. Laslett, L. Smith, and I. Haber, Part. Accel. **13**, 145 (1983).
[18]I. Hofmann, Adv. Electron. Electron Phys. Suppl. **13C**, 49 (1983).
[19]I. Hofmann and J. Struckmeier, Part. Accel. **21**, 69 (1987).
[20]C. Chen and R. C. Davidson, Phys. Rev. Lett. **72**, 2195 (1994).
[21]R. L. Gluckstern, W.-H. Cheng, and H. Yee, Phys. Rev. Lett. **75**, 2835 (1995).
[22]R. L. Gluckstern, W.-H. Cheng, S. S. Kurennoy, and H. Yee, Phys. Rev. E **54**, 6788 (1996).
[23]C. Chen, R. Pakter, and R. C. Davidson, Phys. Rev. Lett. **79**, 225 (1997).
[24]J. Struckmeier and I. Hofmann, Part. Accel. **39**, 219 (1992).
[25]N. Brown and M. Reiser, Phys. Plasmas **2**, 965 (1995).
[26]R. C. Davidson, W. W. Lee, and P. Stoltz, Phys. Plasmas **5**, 279 (1998).
[27]R. C. Davidson and C. Chen, Part. Accel. **59**, 175 (1998).
[28]R. C. Davidson, Phys. Rev. Lett. **81**, 991 (1998).
[29]R. C. Davidson, H. Qin, P. Stoltz, and T.-S. Wang, Phys. Rev. ST Accel. Beams **2**, 054401 (1999).
[30]R. C. Davidson, H. Qin, and P. J. Channell, Phys. Rev. ST Accel. Beams **2**, 074401 (1999).
[31]R. C. Davidson and H. Qin, Phys. Rev. ST Accel. Beams **2**, 114401 (1999).
[32]W. W. Lee, Q. Qian, and R. C. Davidson, Phys. Lett. A **230**, 347 (1997).
[33]Q. Qian, W. W. Lee, and R. C. Davidson, Phys. Plasmas **4**, 1915 (1997).
[34]P. H. Stoltz, R. C. Davidson, and W. W. Lee, Phys. Plasmas **6**, 298 (1999).
[35]H. Qin, R. C. Davidson, and W. W. Lee, AIP Conf. Proc. **496**, 295 (1999).
[36]A. Friedman and D. P. Grote, Phys. Fluids B **4**, 2203 (1992).
[37]S. M. Lund, D. A. Callahan, A. Friedman, D. P. Grote, I. Haber, and T.-S. Wang, ''Theory of an Electrostatic Instability Driven by Transverse-Longitudinal Temperature Anisotropy in Space-Charge-Dominated Beams,'' in *Proceedings of the 19th International Linac Conference* (Chicago, IL, 1998).
[38]I. Haber, D. A. Callahan, A. Friedman, D. P. Grote, S. M. Lund, and T.-S. Wang, Nucl. Instrum. Methods Phys. Res. **A415**, 345 (1998).
[39]I. Haber, D. A. Callahan, A. Friedman, D. P. Grote, and A. B. Langdon, Fusion Eng. Design **32**, 159 (1996).
[40]See, e.g., chaps. 2, 4, 9 and 10 of Ref. 1.
[41]Reference 1 presents a general derivation of the macroscopic fluid Maxwell equations from the Vlasov–Maxwell equations on pp. 22–26. Several aspects of cold-fluid equilibrium and stability properties of nonneutral beam-plasma systems are described on pages 240–276 of Ref. 1.
[42]R. C. Davidson, *Handbook of Plasma Physics–Basic Plasma Physics*, edited by M. N. Rosenbluth and R. Z. Sagdeev (North-Holland, Amsterdam, 1984), vol. 2, pp. 729–819.
[43]R. C. Davidson, B. H. Hui, and C. A. Kapetanakos, Phys. Fluids **18**, 104 (1975).
[44]R. C. Davidson and B. H. Hui, Ann. Phys. (N.Y.) **94**, 209 (1975).
[45]M. Reiser, Phys. Fluids **20**, 477 (1977).
[46]I. Hoffmann, IEEE Trans. Nucl. Sci. **NS-26**, 3083 (1979).
[47]G. A. Krafft, J. W.-K. Mark and T.-S. Wang, SIAM (Soc. Ind. Appl. Math.) J. Appl. Math. **43**, 1390 (1983).
[48]R. C. Davidson, P. Stoltz, and C. Chen, Phys. Plasmas **4**, 3710 (1997).
[49]I. Hofmann, Phys. Rev. E **57**, 4713 (1998).
[50]S. M. Lund and R. C. Davidson, Phys. Plasmas **5**, 3028 (1998).
[51]C. Chen and R. Pakter, Phys. Plasmas **7**, 2203 (2000).